ÇUKUROVA UNIVERSITY
INSTITUTE OF NATURAL AND APPLIED SCIENCES

MSc THESIS

Ahmet Halil ORAN

NUMERICAL INVESTIGATIONS OF CURVED SLANTED SURFACE AND LOWER DEFLECTOR ON THE AHMED BODY

DEPARTMENT OF AUTOMOTIVE ENGINEERING

ADANA-2020

ABSTRACT

MSc THESIS

NUMERICAL INVESTIGATIONS OF CURVED SLANTED SURFACE AND LOWER DEFLECTOR ON THE AHMED BODY

Ahmet Halil ORAN

ÇUKUROVA UNIVERSITY
INSTITUTE OF NATURAL AND APPLIED SCIENCES
DEPARTMENT OF AUTOMOTIVE ENGINEERING

Supervisor : Asst. Prof. Dr. Mustafa Atakan AKAR
Year: 2020, Pages: 65
Jury : Asst. Prof. Dr. Mustafa Atakan AKAR
: Prof. Dr. Mustafa ÖZCANLI
: Asst. Prof. Dr. Ahmet ÇALIK

The effects of passive control models on aerodynamic drag and near wake structures of an Ahmed body with a 25° slant angle was numerically studied. 4 different control methods were studied for this purpose. Curvature control method consists of a curved upper edge of the slanted surface. The radius of the curvature was started from 200 mm and ended at 1000 mm radius. Deflector control method consists of a deflector attached on the lower edge of the slanted surface. Length of these deflectors was started from 1% of the body length and ended at 6% of the body length. Later on, based on the best-resulted curvature and deflector control models, a new control model created and called the optimum control method. Lastly, a deflector was relocated on the slanted surface and the deflector end was aligned to the end of the body vertically. Simulations were conducted in Fluent (19.1) software at 60 m/s inlet velocity, which it was equal to Reynolds number = 4.2×10^6. The obtained results and displayed flow structures were compared with the base Ahmed body result. As a result of these simulations, the coefficient of drag was reduced up to 21.16%.

Key Words: Drag Coefficient, Lift Coefficient, Ahmed Body, CFD

ÖZ

YÜKSEK LİSANS TEZİ

AHMED GÖVDESİ ÜZERİNDEKİ KAVİSLİ EĞİMLİ YÜZEYİN VE ALT SAPTIRICININ SAYISAL ARAŞTIRMALRI

Ahmet Halil ORAN

ÇUKUROVA ÜNİVERSİTESİ
FEN BİLİMLERİ ENSTİTÜSÜ
OTOMOTİV MÜHENDİSLİĞİ ANABİLİM DALI

Danışman : Doç. Dr. Mustafa Atakan AKAR
Yıl: 2020, Sayfa: 65
Jüri : Doç. Dr. Üyesi Mustafa Atakan AKAR
: Prof. Dr. Mustafa ÖZCANLI
: Doç. Dr. Ahmet ÇALIK

Pasif kontrol modellerinin, 25° eğik açılı bir Ahmed modelinin aerodinamik sürtünme ve girdap yapıları üzerindeki etkileri sayısal olarak incelenmiştir. Bu doğrultuda 4 farklı kontrol yöntemi üzerinde çalışılmıştır. Kavis kontrol yöntemi, eğimli yüzeyin üst kenarına uygulanan kavisten oluşur. Bu kontrol yönteminde, eğrilik yarıçapı 200 mm'den başlayarak 1000 mm yarıçapında sona ermiştir. Deflektör kontrol yöntemi, eğimli yüzeyin alt kenarına yerleştirilmiş bir deflektörden oluşur. Bu deflektörlerin uzunluğu gövde uzunluğunun %1'inden başlamış ve gövde uzunluğunun %6'sında sona ermiştir. Daha sonra en iyi sonuçları veren kavis ve deflektör kontrol modelleri birleştirildi ve optimum kontrol yöntemi olarak adlandırıldı. Son olarak, eğimli yüzey üzerinde deflektörün bitimi gövdenin bitimi ile aynı hizada olacak şekilde konumlandırıldı. Simülasyonlar Fluent (19.1) yazılımında, Reynolds sayısının 4.2 x 10^6 'ya eşit olduğu 60 m/s giriş hızında gerçekleştirilmiştir. Elde edilen sonuçlar ve gösterilen akış yapıları, Ahmed gövdesinin sonuçları ile karşılaştırılmıştır. Bu simülasyonların sonucu olarak, sürtünme katsayısı %21.26 oranına kadar düşmüştür.

Anahtar Kelimeler: Sürtünme Katsayısı, Kaldırma Katsayısı, Ahmed Body, CFD

EXTENDED ABSTRACT

For vehicle aerodynamics, one of the most important research subject is aerodynamic drag, which is directly related to fuel efficiency. Fuel costs, environmental issues and the truth that fossil fuels will run out in the future, encourages us to make more fuel-efficient vehicles. Besides fuel efficiency concerns also handling is very important for ground vehicles. Especially at high speed, lift force becomes an important criterion for us.

To reduce drag and lift coefficient, we need to understand flow structures on a vehicle. Because of ground vehicles have detailed geometries, its hard to investigate both experimental and numerical these flow structures. Also, the different exterior design of these vehicles makes it difficult to compare flow control applications' contributions. For this reason, we need a simplified vehicle model. In line with this need, Ahmed et al. introduced a model in 1984.

For ground vehicle bodies, drag is mainly caused by pressure drag. In their experimental research, Ahmed et al., (1984) showed that up to 85% of the total drag was directed by pressure drag and more than 75% of the pressure drag was due only to the averaged force applied on the rear part of the model. The location of the flow separation at the rear part of the model determines the structure of the wake flow and the size of the separation zone presents a major contribution to the drag. In this study, we try to avoid this separation or its impossible moving away from these structures from the rear part of the model.

To maintain this, we applied a curvature to the upper edge of the slanted surface. The radius of the curvature was started from 200 mm and ended at 1000 mm radius.

After this control method, for the move away from these structures from the rear part of the model, we attached a deflector on the lower edge of the slanted surface. The length of these deflectors was started from 1% of the model length and ended at 6% of the body length.

Later on, based on the best-resulted curvature and deflector control models, a new control model created and called the optimum control method. Lastly, a deflector was relocated on the slanted surface and the deflector end was aligned to the end of the body vertically. Simulations were conducted in Fluent (19.1) software at 60 m/s inlet velocity, which it was equal to Reynolds number = 4.2×10^6. Mesh quality is very important in CFD analysis. Mesh quality affects many important outputs from the number of steps from which the results be obtained to the analysis result. For this reason, it is essential to create quality mesh. For that purpose, different unit sizes were assigned to the surfaces of the model and tetrahedral mesh structure applied. These unit sizes were set to be 2.5 mm and 5 mm, and minimum unit sizes were assigned between 0.1 mm and 0.5 mm. The smaller 2.5 mm unit sizing was used on the forehead, slanted surface and back end of the model. Precise and sufficient inflation layers must be used in the mesh generation to solve the boundary layer correctly. Therefore, different first layer heights were applied to provide the condition of $30 < y+ < 100$ Huminic, (2017). This inflation was applied in 7 layers and the first layer thickness was applied between 0.31 mm and 2.91 mm.

The obtained results and displayed flow structures were compared with the base Ahmed body result. As a result of these simulations, the coefficient of drag was reduced up to 21.16%.

ACKNOWLEDGEMENTS

I would like to represent my sincere thanks to my supervisor Assoc. Prof. Dr. Mustafa Atakan AKAR for his advice, guidance, understanding and support during the preparation of this thesis.

My thanks are extended to Res. Asst. Oğuz BAŞ for providing invaluable research advice and motivation during my thesis.

Last but not the least, I have my deepest appreciation to my beloved family for their understanding and endless support during the preparation of this thesis.

CONTENTS **PAGE**

LIST OF FIGURES **PAGE**

NOMENCLATURE

α	: Angle of the slant
l, L	: Length of the Ahmed body
w	: Width of the Ahmed body
C_d	: Coefficient of drag
C_l	: Coefficient of lift
C_p	: Coefficient of pressure
1000R	: 1000 mm radius applied curvature control model
d6	: Deflector with 6% of Ahmed body's length
op6	: Optimum control model with 6% deflector length
rl6	: Relocated deflector control model with 6% deflector length
t	: Time
u, v, w	: Velocity Components
ρ	: Density

1. INTRODUCTION

1.1. Vehicle Aerodynamics

In-vehicle aerodynamics one of the most important research subjects is aerodynamic drag, which is directly related to fuel efficiency. Because of increasing fuel cost trend, environmental issues and the truth that fossil fuels will run out encourages us to make more efficient vehicles. Besides fuel concerns also driveability is important, which indicates the importance of the lift force.

To optimize these features, the design of the vehicle and engineering are key points. To reduce drag and improve handling we have to understand of flow structures of vehicles. Since real ground vehicles have complex geometry it is hard to investigate them with both experimental and numerical methods because of their complex flow structures. Also, because of their different designs, it is hard to understand real contributes to flow control applications.

While vehicle manufacturers are developing new models, the design of the model mostly becomes apparent in the early stages of development in line with the class and the features it will have. Since this development process is limited and costly, the improvement to be made should be completed in a short time and must be economical. In this respect, it is useful to make aerodynamic improvements by numerical methods (CFD). CFD is very advantageous in terms of the fewer installation costs in the work to be done and the ability to prepare and test the changes in the model more easily. While providing these benefits, it is very important to choose the correct analysis method so that the analysis can yield consistent results.

Nowadays, geometries of ground vehicles have become quite detailed and differ from each other. Which, makes it very difficult to compare the work with another. For this reason, there is a need for a simple shaped generic model body that can meet the basic aerodynamic needs of the ground vehicle. In line with this need, Ahmed et al. introduced a model in 1984.

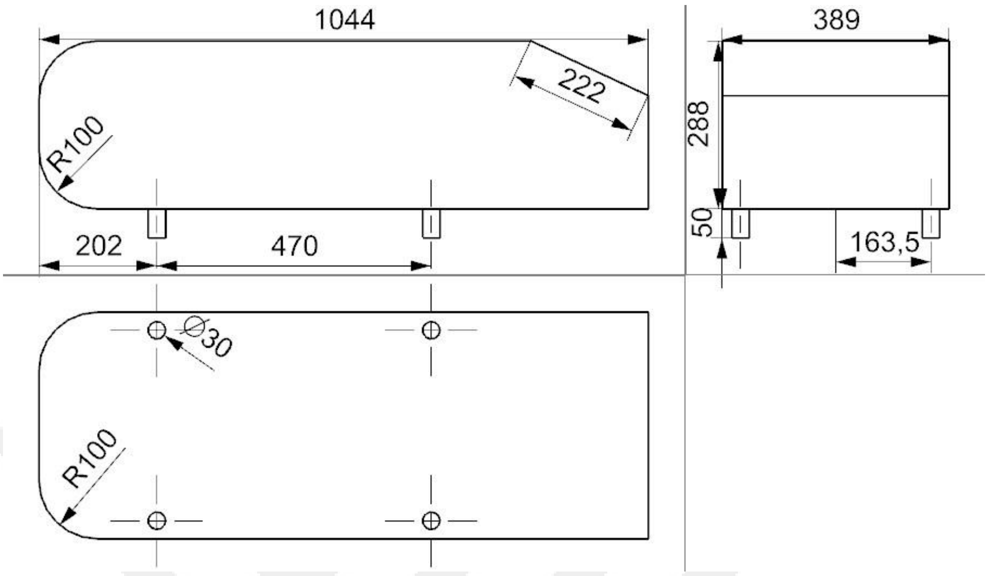

Figure 1.1. Form and measurements of the car model used in this study, from Ahmed et al. (1984).

The original Ahmed body used in the Ahmed et al., (1984) experiments, has dimensions of height 288 mm, length 1044 mm and width 389 mm. The length of the slanted surface is 222 mm, whatever the angle α. The ground clearance of the Ahmed body is 50 mm. This geometry is represented in the figure above.

Since this model geometry produces the same flow structures as real ground vehicles, it is used as a reference in studies that examine flow structures. The front of the Ahmed body contains 1/4 cylindrical surfaces to prevent flow separations. To understand the flow structure on the back of the Ahmed body, both experimental and numerical studies have been done. As Hanfeng et al., (2016), pointed out in their study, there are 3 main components at near wake flow: The longitudinal vortices on the side edges of the slanted surface, the recirculation bubble on the slanted surface and the recirculation torus on the base of the model.

The flow around the model significantly influenced by the angle of the rear slanted surface. In the first regime; (α below 12.5°) the flow flowing over the model remains completely attached to the back surface, and a longitudinal vortex pair appears in close decomposition. The drag coefficient was about 0.25 and it was almost independent in terms of this order Strachan et al., (2007). In regime 2,(α between 12.5° - 30°) the flow on the slanted surface becomes mostly 3 dimensional. Compared to the first regime, the traces of the longitudinal vortexes are much stronger. Also, there was a significant increase in C_d because the main pressure drops considerably, Vino et al., (2005). In the third regime, (α above 30°) the flow on the model can no longer be reattached down the slanted surface. The near-constant pressure of the flow was above the pressure of the entire slanted surface. This leads to a significant decrease in the drag coefficient and also the strengthening of the trail vortexes. This shows us that most of the aerodynamic drag occurs due to the three-dimensional vortex dissociation on the slanted surface.

Unlike the other vehicles such as aircraft and ships, in bluff bodies drag is mainly caused by pressure drag, not because of friction. In their experimental research, Ahmed et al., (1984) showed that up to 85% of the total drag was directed by pressure drag and in some model configurations, more than 75% of the pressure drag was due only to the averaged force applied on the rear part of the model while only 9% was due to the force applied on the front of the model Beaudoin et al., (2004). The location of the flow separation determines the structure of the wake flow and the size of the separation zone presents a major contribution to drag. So, avoidance of separation or, if this is impossible, its control is the most significant objective of ground vehicle aerodynamics, Hucho & Sovran, (1993).

Different control methods are needed as flow structures will change according to the slant angle of the Ahmed body. There are both active and passive control techniques that can use today to control these flow structures. Active control methods require energy input from the outside when controlling the flow. On the other hand, there is no energy input in passive control methods and it is easier to apply. These passive control methods consist of geometrical additions or modifications to manage the flow.

1.2. Objectives of Present Investigation

The main aim of this research is; on the body revealed by Ahmed et al., (1984), examine the effects of the passive control method chosen on the drag and lift coefficients. For this purpose, the effects on the flow were examined by adding and rounding different length deflectors to the upper and lower edges of the back end of the body as the flow control method. Thus, the effects of these modifications on drag and lift coefficients were investigated defined. Understanding the effects of these changes on flow may enable vehicles to be improved aerodynamically.

A 1:1 scale Ahmed body with additions employed as a simulation case. These control models were investigated through the CFD numerical method.

1.3 Outline of the Study

The outline of the thesis, as follows. It was structured in five chapters. The background and objectives of the present investigation have been presented in Chapter 1.

Chapter 2 summarizes the literature survey and unresolved issues for the ground vehicle aerodynamics.

Chapter 3 describes the domain setup, body design and numerical method employed throughout the investigation. The simulation details, for example, computational setup and grids employed were described.

Results and discussion of numerical calculations (using k-ω SST method) of the flow around the Ahmed body was presented in Chapter 4. Flow visualizations and turbulent coherent structures were discussed.

Finally, Chapter 5 summarizes the main findings and conclusion of the present work and provides recommendations for further investigations as future works.

2. PREVIOUS STUDIES

At the beginning of the 20th century, motor vehicles started to enter people's life for the first time, and the aerodynamic properties of these vehicles were ignored. Unfortunately, there wasn't aerodynamic concern about the earliest car. Because of the limited technology in the automotive industry and poor roadway conditions, aerodynamic benefits could not be achieved in ground vehicles and were not required. Take a look at Ford's unique Model T it looks like a horse carriage more than a car, a very boxy design. Most of the early cars didn't need to worry about aerodynamics because they were relatively slow.

Aerodynamic application on ground vehicles in the following years began after the important achievements in aeronautical aerodynamics. Body shapes used in aviation and whose aerodynamic benefits have been proven have been applied to land vehicles in the same way, almost unchanged. However, these aerodynamic forms which come from aviation caused unwanted aesthetic appearances in ground vehicles, Hucho & Sovran, (1993).

In the coming years, as the engines became more powerful so cars became faster, engineers realized that wind resistance applied to car considerably limited their speed. Significant achievements in the aerodynamic development of ground vehicles were listed by Bayraktar, (2002) following order.

- Klemperer observed that the flow pattern changed significantly with the half-body brought closer to the ground.
- Kamm et al. (1934) and Koenig-Fachsenfeld (1951) studied the effect of the flow by cutting the rear end of the body.
- Hucho et al. (1976) introduced the development as 'detail-optimization' by making changes to small components on the vehicle. Thanks to details such as the radius of edges and pillars, spoiler size and position, significant conclusions were obtained.

- Morel (1978) and Ahmed et al. (1984) studied the flow patterns behind the simplified vehicle model they identified.
- Han (1989) performed numerical solution methods (CFD) to ground vehicle aerodynamics.
- Nowadays, aerodynamic design analysis is important in the application of parts such as side mirrors, air curtains, air deflectors and wings to passenger cars, heavy vehicles and racing vehicles.

Aerodynamics became an important point for engineers as the engines got more powerful in the 1930s. The aeronautic design approach started to be implemented in models of that period. However, these design applications did not visually appeal to people and reduced the practicality of the vehicle. Therefore, engineers began to examine the effects of the configurations made in the front and rear areas of the ground vehicles on the flow.

By the end of the '30s, the designs of the models were influenced by the streamlined approach. In the following years, the classic design concept meant more than aerodynamic concerns. Some compelling reasons pushed automakers into this conservative approach. Some of these were V8 engines with high power potential with visual prestige, spacious interior and luggage capacity desire, traditional RWD layout and cheaper fuel prices. Over time, reasons such as fuel costs, economy and progressive attitude in Europe have combined smaller vehicles with an aerodynamic design. This new design concept has benefited efficiency and affordability. Of course, racing organizations that gained momentum in the post-war period also contributed to aerodynamic gains.

When we came to the '70s, the world-wide oil crisis put pressure on automobile manufacturers to improve their fuel economy. Thanks to this, manufacturers have taken a big step in improving the aerodynamics of land vehicles.

Vehicle designers have developed various design strategies to achieve the lowest coefficient of drag as much as possible.

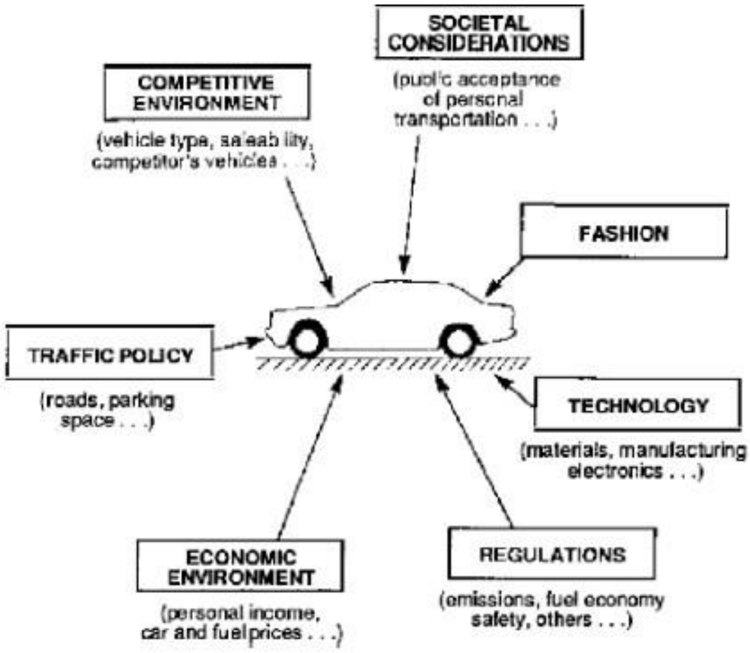

Figure 2.1. Factors that influence the concept of a car (Hucho and Sovran,1993)

2.1. Ground Vehicle Aerodynamics

In real life, automobiles are difficult to model or work on experimentally due to their complex and detailed designs. Besides, the use of bodies with different models in aerodynamic studies will make it difficult to understand the contribution of the study to the flow. Thus, a simplified geometry should be used that can reveal the basic characteristics of ground vehicle aerodynamics. In this direction, Le Good & Garry, (2004) review the design characteristics and use of several key reference models. Its seen that there was one bluff body geometry generally used in the literature thanks to its basic shape and ease of operation with. This bluff body named as Ahmed body, which used in this study. Morel, (1978), proposed a bluff body that meets this criterion for use in ground vehicle aerodynamics and then this bluff body geometry was revised by Ahmed et al., (1984). Ahmed et al., (1984), directed extensive research about the characteristics of flow around this generic bluff body.

Ahmed et al., (1984), have enquired the characteristics of flow through the rear end of the bluff body model and reported drag coefficient change.

Ahmed body has 1044 mm length, 288 mm height and 389 mm width. The length of the slanted surface is 222 mm, whatever the angle. The ground clearance of the Ahmed body is 50 mm. Although its forms are free from all accessories as well as from wheels, it still retains the primary behaviour of the vehicle aerodynamics.

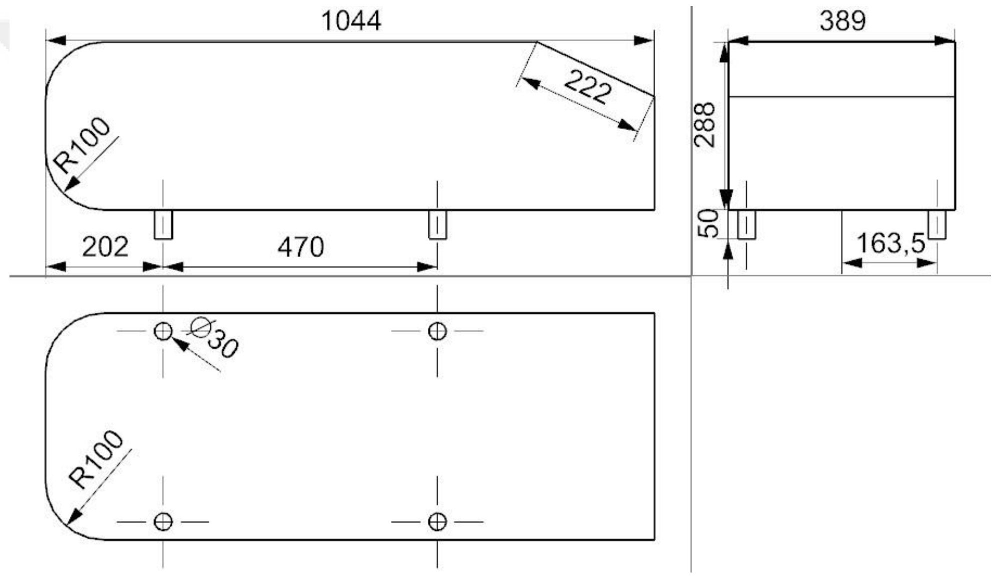

Figure 2.2. Dimensions of the Ahmed Body

Ahmed et al., (1984), have executed experiments along with different slant angles and defined the properties of the flow for these angles. The most significant acquisition from their work is that the main source of body drag was because of pressure drag at the rear end. The effects of the slant angle to the coefficient of drag are shown in Figure 2.3.

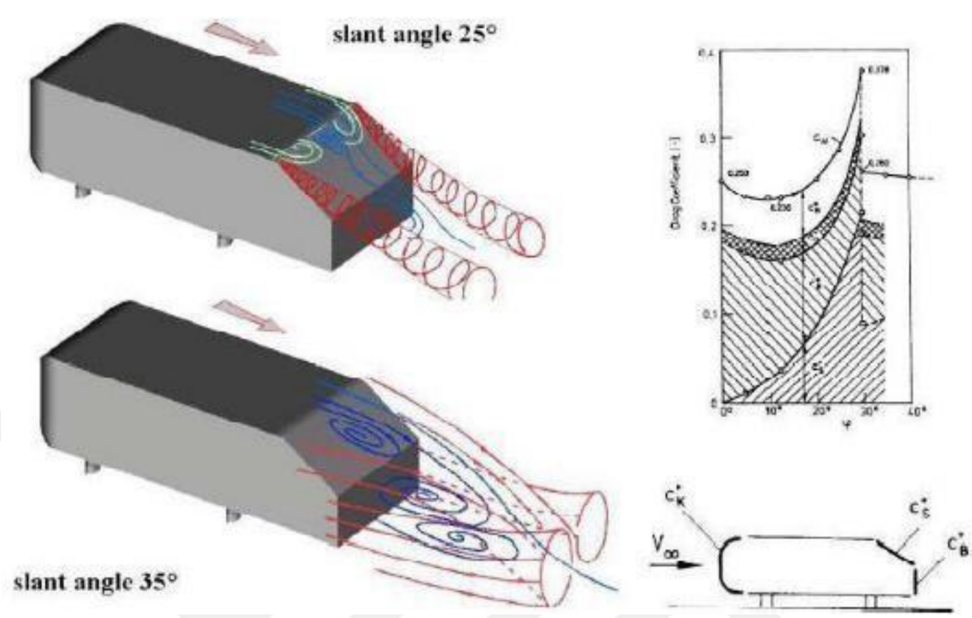

Figure 2.3. Flow generation on the rear end of the Ahmed body for 25 and 35° (left; Lienhart et al., 2000) and dependence of drag coefficient on slant angle α (right; Ahmed et al., 1984)

Hanfeng et al., (2016), enquired experimentally efficacious of deflectors on the drag coefficient and near wake of an Ahmed model with a 25° slant. They placed deflectors at the side edges and upper edge of the slanted surface and conducted experiments in a closed-circuit low-speed wind tunnel Reynolds number of $8.7\text{x}10^5$. As a result, when the length of the 1% of Ahmed Body, deflector placed at the side edges of the slant its effects on the near wake are negligibly small and the corresponding drag was increased slightly, compared to the uncontrolled flow. With the deflector length increased to 2% and 3% of Ahmed body, the D-shape separation bubble and the trailing vortices were noticeably suppressed, with the drag reduction reaching 3.5% and 7.2%, respectively.

Fourrié et al., (2011), experimentally investigated passive flow control on Ahmed Body. This control method was a deflector, fitted on the upper edge of the slanted surface. They found out drag reduces up to 9% were obtained depending on the deflector angle. According to the study, this decreasing occurs due to wide separated region. This wide separated region disrupts the development of the counter-rotating longitudinal vortices appearing on the lateral edges of the slanted surface.

Ha et al., (2011) have conducted drag reduction simulations by rear deflector on a truck. When deflector positioned at the back end of the roof, the deflector increased the cabin back surface pressure coefficient. Thus, the attachment of the rear flow to the tailgate region was eliminated. Their research showed a coefficient of drag was reduced with increscent deflector length and negative angle despite the expanded backflow in the wake. However, the coefficient of drag did not decrease any further after a particular negative angle.

Guilmineau, (2008), has investigated numerically the flow around the Ahmed body for the rear slant angles of 25 and 35°. In his study, in 35° slant case the two-dimensional behaviour of the flow was well estimated, however, the transition of the wake to a fully three-dimensional, for the slant angle 25, was not reproduced. For this reason, the flow around the Ahmed body with 25 slant angle case can be noted as an open issue for turbulence modelling.

Beaudoin & Aider, (2008), have put forward an experimental study on passive control over an Ahmed body. This passive flow control was accomplished through deflectors fixed on every edge around the slanted and rear flat surfaces of the model. Deflectors were had variable angle values compared to walls. Parametric experiments show that the most efficient configuration for the deflectors are along the side edges of the rear slanted surface, i.e. in the area where longitudinal vortices are created, and also at the juncture between the roof and the rear slanted surface, where the flow separates. They also found out accretive effects between leading to -25% drag reduction and -105% lift reduction by the combinations of different deflector arrangements.

Raina et al., (2017), presented a numerical study of drag reduction technique based on a passive control method around an Ahmed body. This method was a deflector located at the upper edge of the slanted surface. The effect of the deflector was investigated to determine the specific angle at which maximum potential drag decrease can be achieved. In this study, deflectors angles were varied between -25 - +60° and inlet velocity was 16 m/s and 40 m/s. As a result of the study, a 7% decrease in the coefficient of drag was acquired compared to the case when there is no deflector.

Pujals et al., (2010), have put forward an experimental study to try to reduce the coefficient of drag. They indicated flow separation on the back of the Ahmed body is suppressed by large-scale traces from the ceiling of the model. Therefore, to provide flow control, they experimentally examined the effects by adding cylindrical elements to the ceiling. The experiments were carried out for Velocity = 20 m / s on Ahmed body with a 25° slanted surface angle. As a result, they achieved up to 10% drag coefficient reduction thanks to the modifications.

Thacker et al., (2012), examined the separated flow on the Ahmed body with a 25° slanted surface. The experiment they carried out consisted of analyzing the effect on different structures that developed after separation on the slanted surface. They used two different models to reduce the drag coefficient and better understand the flow properties. While the first of these models were the standard Ahmed body, the other one has rounded edge at the top of the rear slanted surface with a radius of 80 mm. Different wake structures were experimentally analyzed and compared with each other. In the comparisons between these two models, they found that the drag coefficient decreased by 10% while the lifting coefficient remained the same. They found that the absence of a separation bubble on the rear slanted surface strongly affected the near rear wake of the body, contributing to the reduction of the coefficient of drag.

Altaf et al., (2014), aimed to reduce the drag coefficient with passive control methods for heavy vehicles in their CFD studies. In their work, they achieved a baseline drag coefficient for comparison by making base work on the simplified MAN TGX series truck. All the deflectors they were placed for passive flow control are positioned at an angle of 50° and they tested various lengths of these 3 main deflector forms in simulation. As a result, they achieved a maximum drag reduction of 11.1% with an elliptical deflector of 0.12 m length.

As stated above, studies on passive flow control methods are promising to improve aerodynamic performance.

3. MATERIAL AND METHOD

3.1. Geometry

As mentioned earlier, this study was based on the model that represents a basic ground vehicle model which firstly introduced by Ahmed et al., (1984). In order to understand the aerodynamic behaviour of the ground vehicles, by considering the previous studies decided to use this model. As stated in the previous sections, the aerodynamic properties of Ahmed Body are highly influenced by the angle of the rear slanted surface. All analyses carried out in this study was performed on Ahmed Body with a 25° rear slant angle.

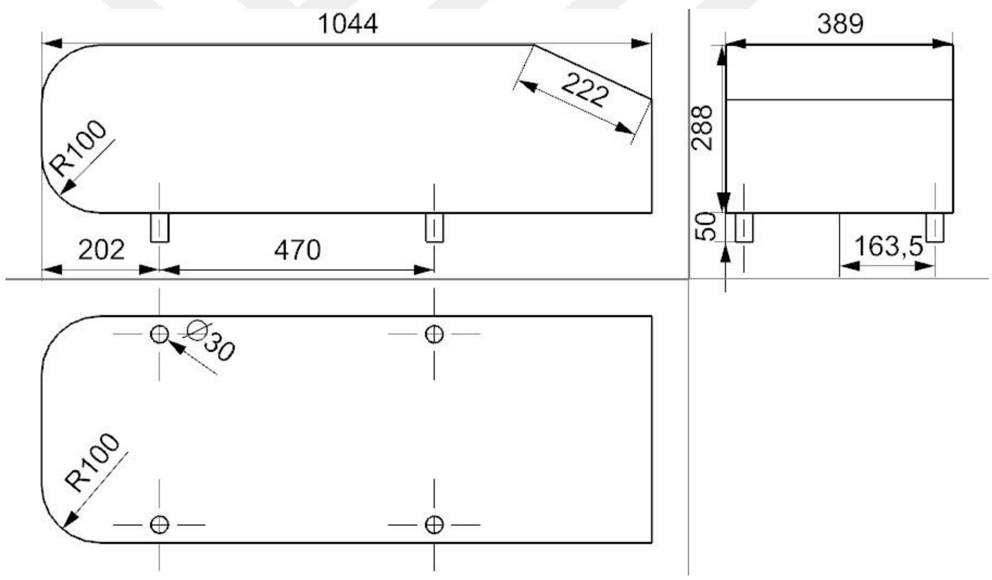

Figure 3.1. Ahmed body dimensions

Since the longitudinal vortices and the separation bubble formed behind the model are effective in the drag coefficient generated by the Ahmed body is known. By moving further these recirculation structures formed on the rear end of the model, the drag coefficient can be decreased. Therefore, to reduce the coefficient of drag, controls that can move further these circulation structures away from the back of the model have determined.

3.1.1. Curvature Control Method

The first of these controls was to apply curvature in the Radius of 200, 400, 600, 800 and 1000 mm (200R, 400R, 600R, 800R and 1000R) to the upper edge of the rear slanted surface. These curvature applied bodies shown below.

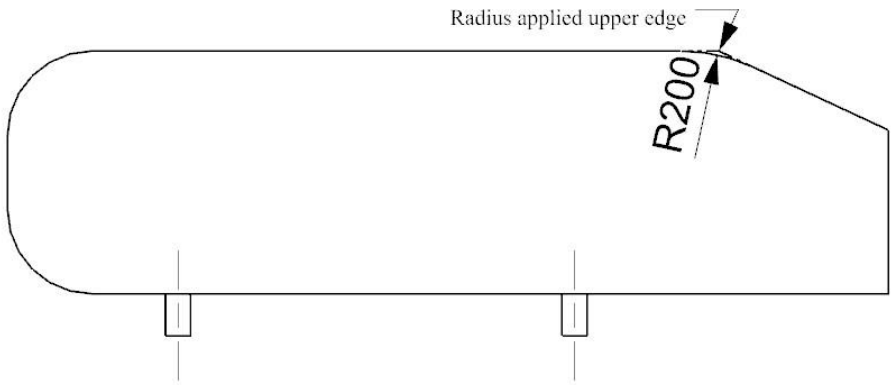

Figure 3.2. Side view of the 200 mm radius curvature control method

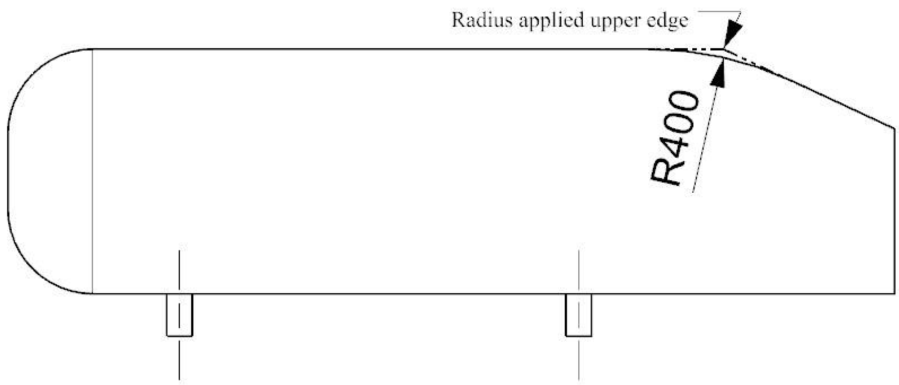

Figure 3.3. Side view of the 400 mm radius curvature control method

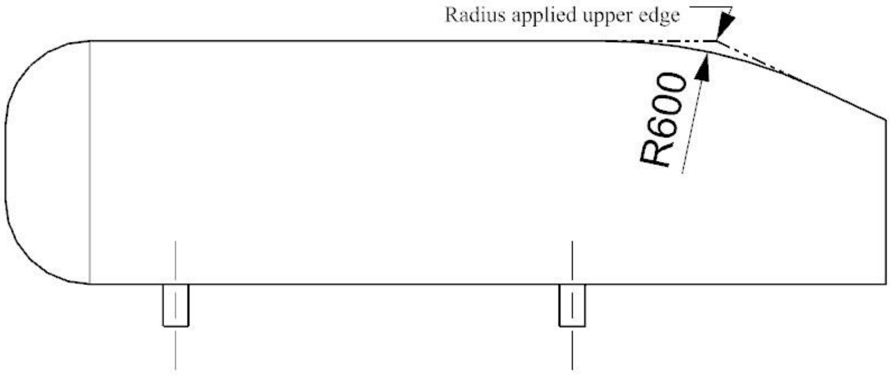

Figure 3.4. Side view of the 600 mm radius curvature control method

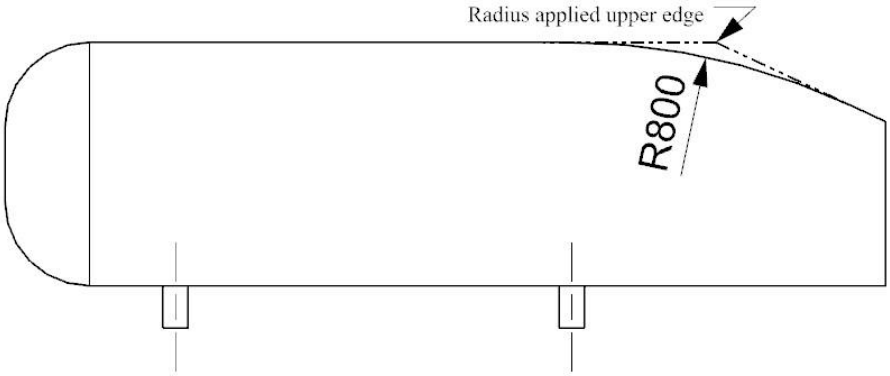

Figure 3.5. Side view of the 800 mm radius curvature control method

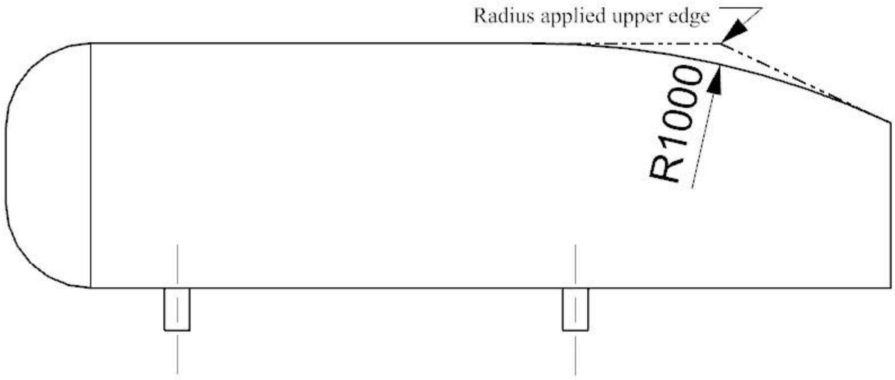

Figure 3.6. Side view of the 1000 mm radius curvature control method

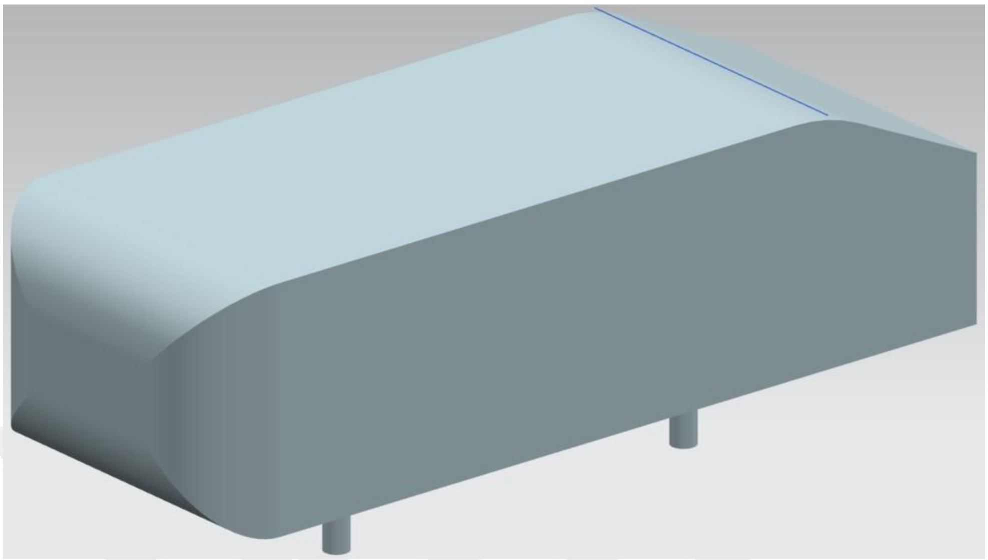

Figure 3.7. Isometric view of curvature control method

3.1.2. Deflector Control Method

Secondly, deflectors with lengths of 1, 2, 3, 4, 5 and 6% (d1, d2, d3, d4, d5 and d6) of the model length are added to the lower edge of the rear slanted surface. All of these deflectors are 10 mm thick and their outer edges are cut 45°. These deflector attached bodies shown below.

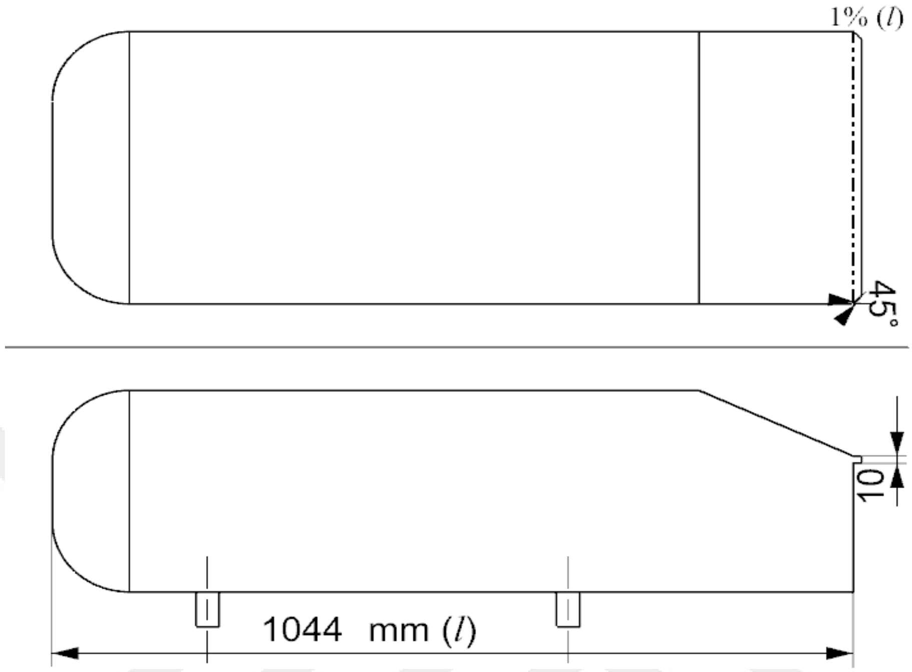

Figure 3.8. Top and side view of the 1% deflector control method

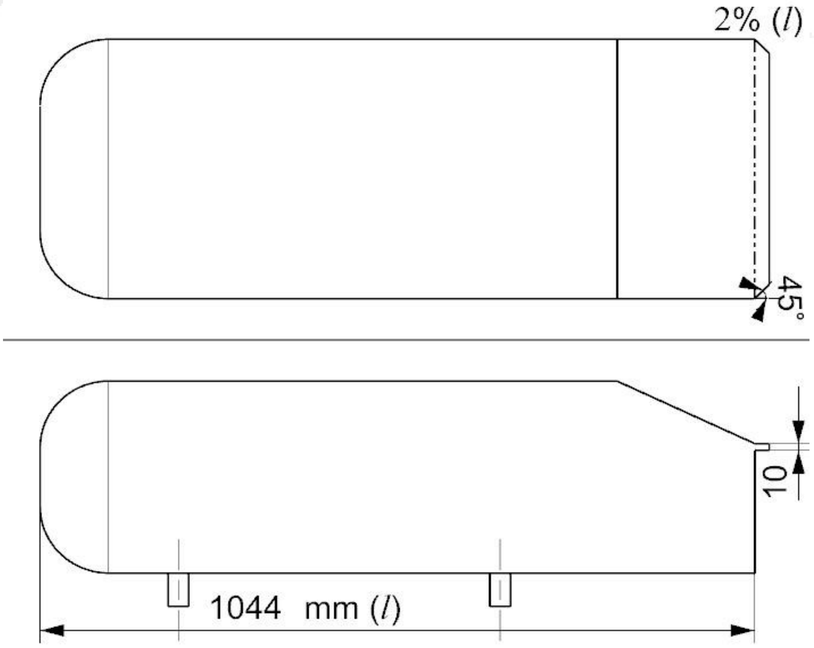

Figure 3.9. Top and side view of the 2% deflector control method

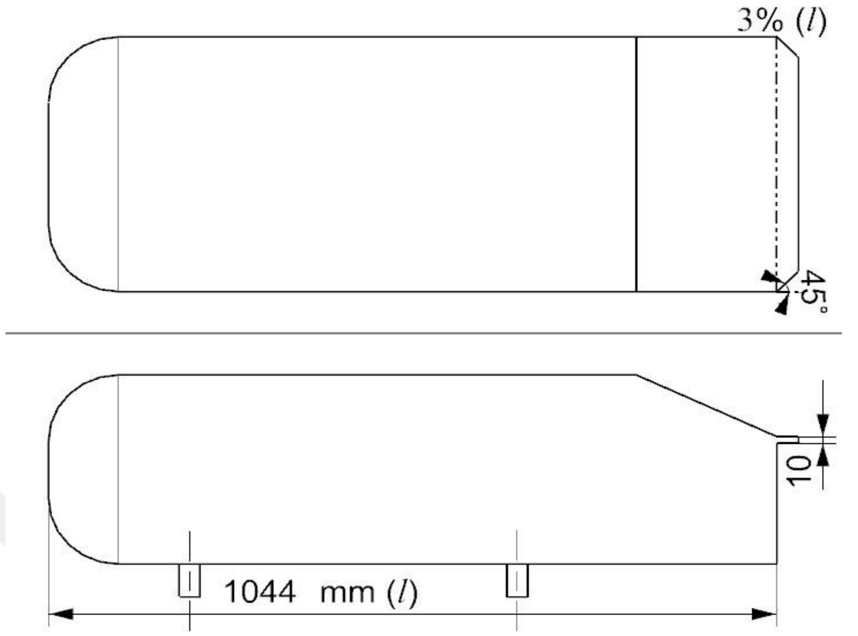

Figure 3.10. Top and side view of the 3% deflector control method

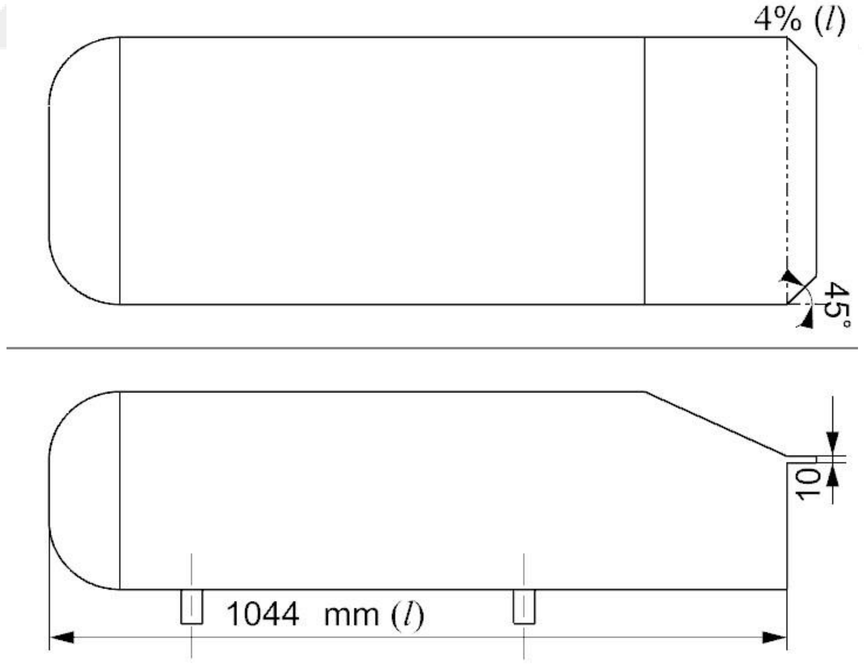

Figure 3.11. Top and side view of the 4% deflector control method

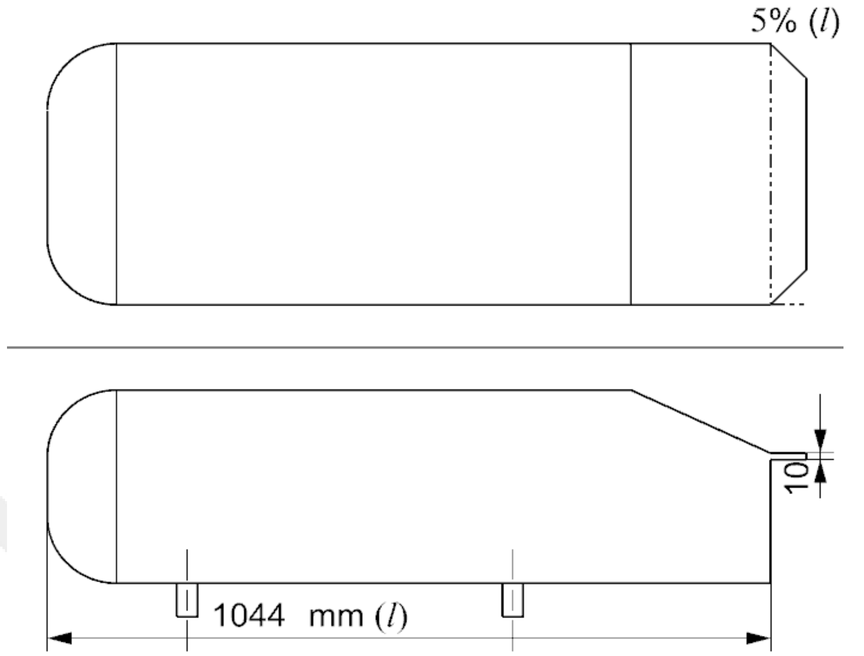

Figure 3.12. Top and side view of the 5% deflector control method

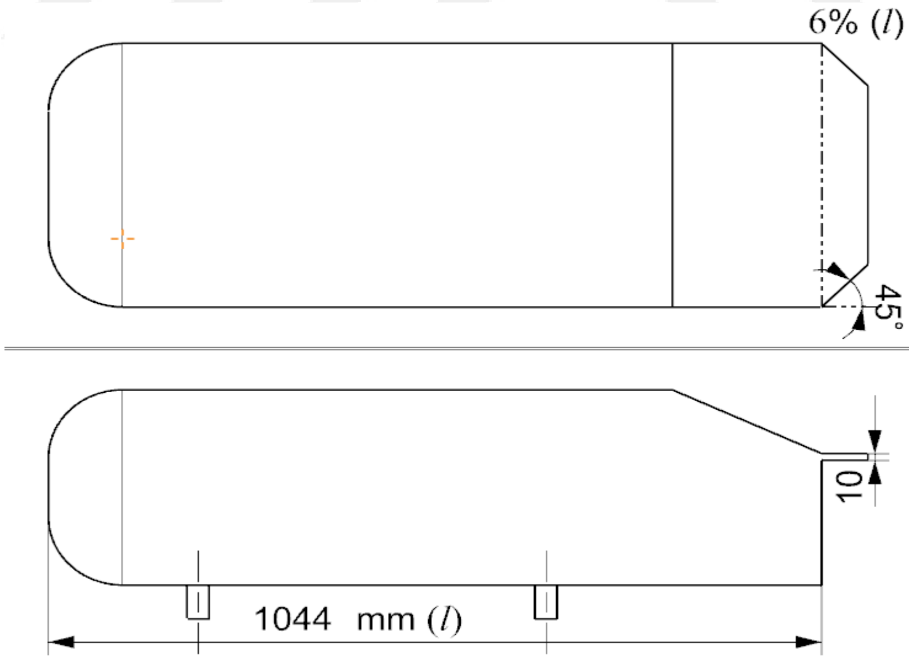

Figure 3.13**.** Top and side view of the 6% deflector control method

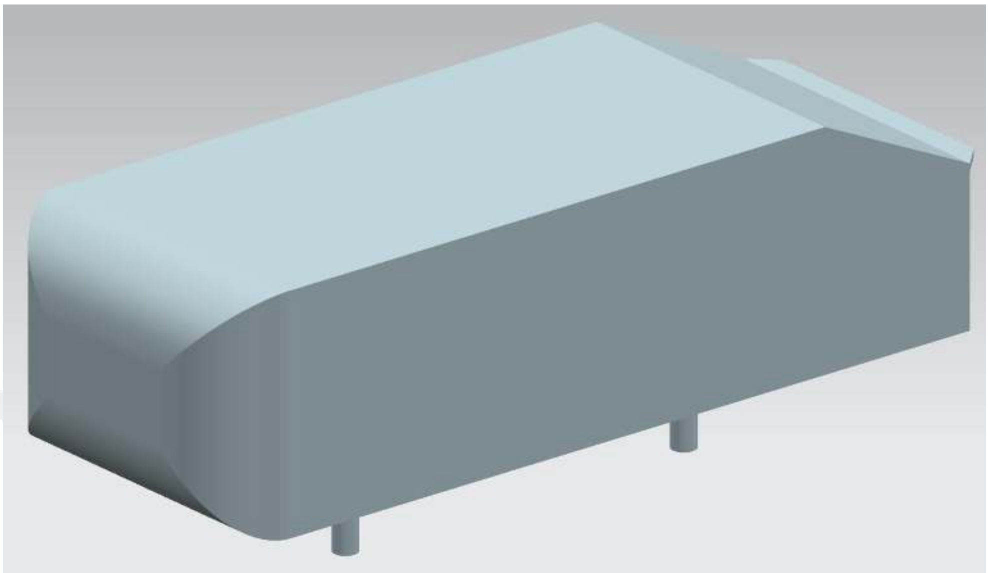

Figure 3.14**.** Isometric view of deflector control method (3% deflector)

3.1.3. Optimum Control Method

In this control model, based on the best-resulted curvature and deflector control models, a new control model created and called the optimum control method. This optimum control model is shown below (it was named shortly as op6 in next chapters).

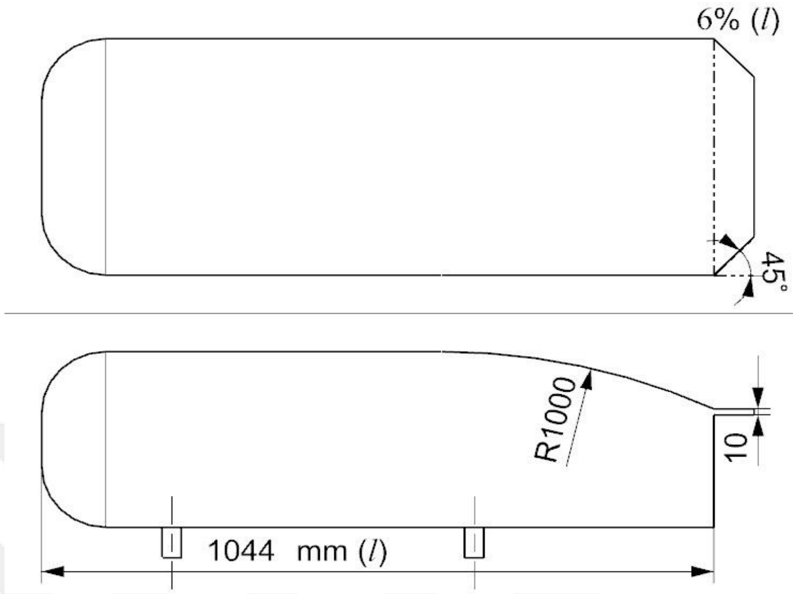

Figure 3.15. Top and side view of the optimum control method

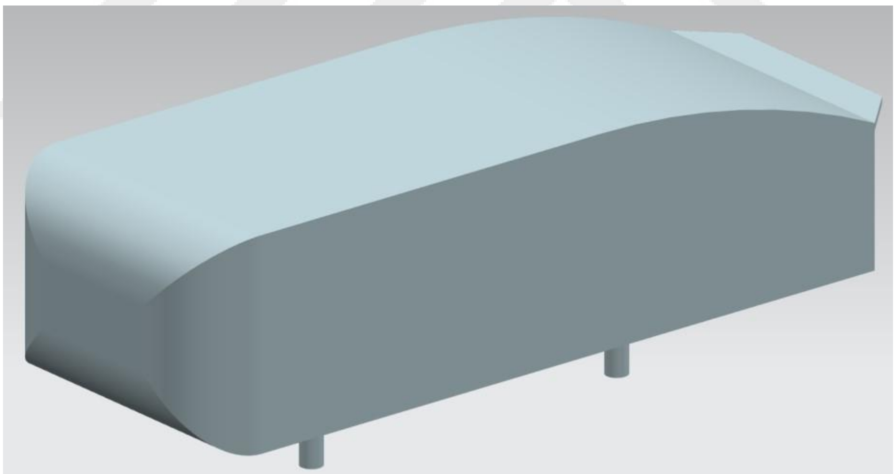

Figure 3.16. Isometric view of optimum control method

3.1.4. Relocated Deflector Control Method

In real life, the class those models are associated with has dimensional limits. The aerodynamic effects of the deflector control, when positioned without exceeding the size limits of the model, was examined. In this last control method, the deflector control, which gives the best aerodynamic result, was repositioned on the rear slanted surface, ending in line with the rear end face of the model. This relocated deflector method is shown below (it was named shortly as rl6 in next chapters).

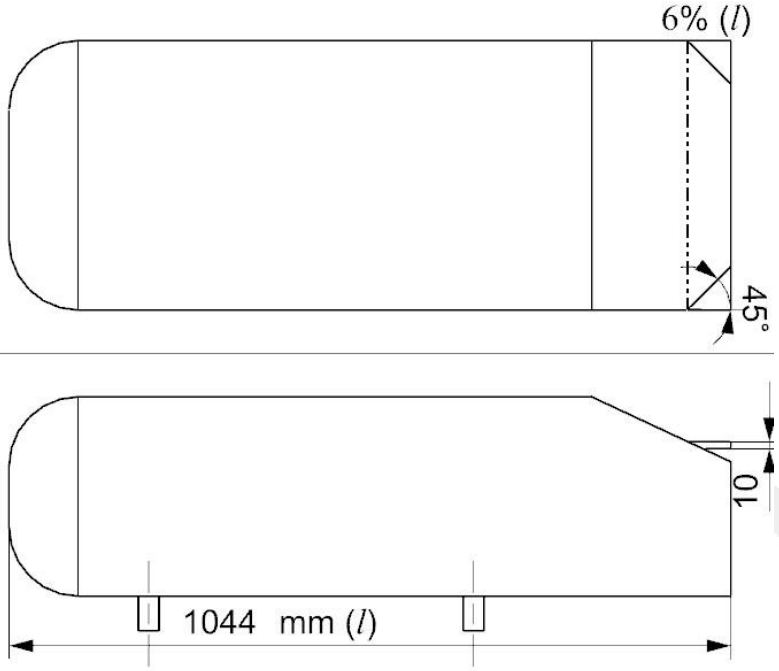

Figure 3.17. Top and side view of relocated deflector control method

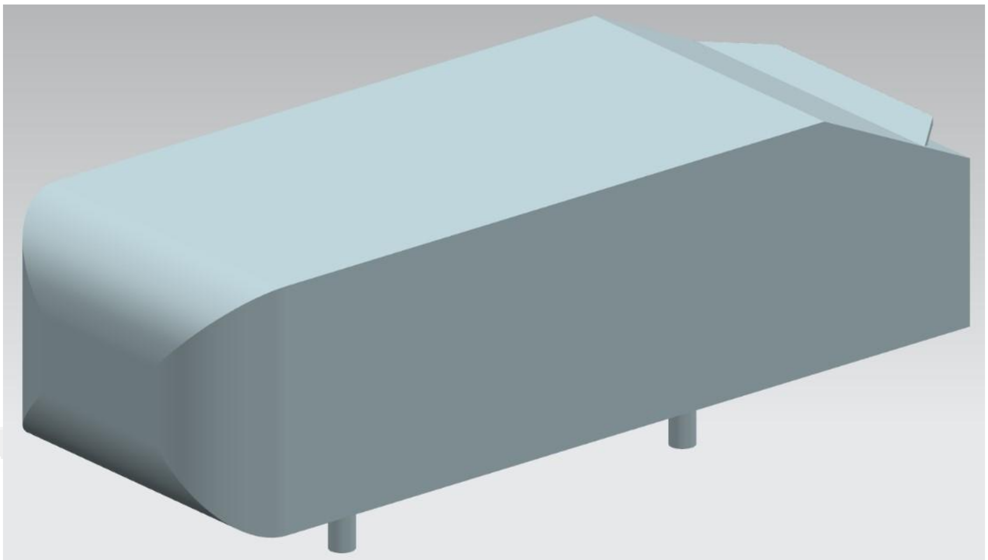

Figure 3.18. Isometric view of relocated deflector control method

All these control geometries were prepared in Siemens NX (version 12.0) program.

3.2. Mesh Generation

All of the CFD simulations were completed in ANSYS Fluent (version 19.1) program. Mesh quality is very important in CFD analysis. Mesh quality affects many important outputs from the number of steps from which the results be obtained to the analysis result. For this reason, it is essential to create quality mesh. For that purpose, different unit sizes were assigned to the surfaces of the model and tetrahedral mesh structure applied. These unit sizes were set to be 2.5 mm and 5 mm, and minimum unit sizes were assigned between 0.1 mm and 0.5 mm. The smaller 2.5 mm unit sizing was used on the forehead, slanted surface and back end of the model. Computational domain in mesh display shown below, Figure 3.19.

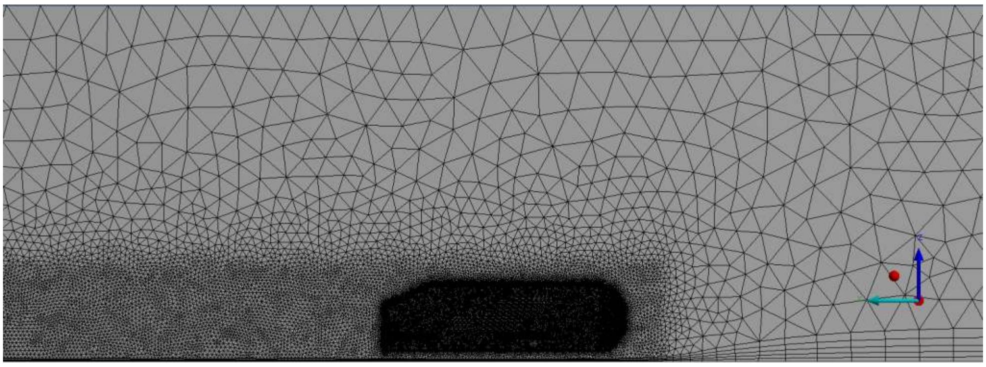

Figure 3.19. Mesh display

Precise and sufficient inflation layers must be used in the mesh generation to solve the boundary layer correctly. Therefore, different first layer heights were applied to provide the condition of 30 <y + <100 Huminic, (2017). This inflation was applied in 7 layers and the first layer thickness was applied between 0.31 mm and 2.91 mm. After obtaining this intended interval in uncontrolled analysis, obtaining of this interval continued in the control model analyses. y+ monitor was shown below.

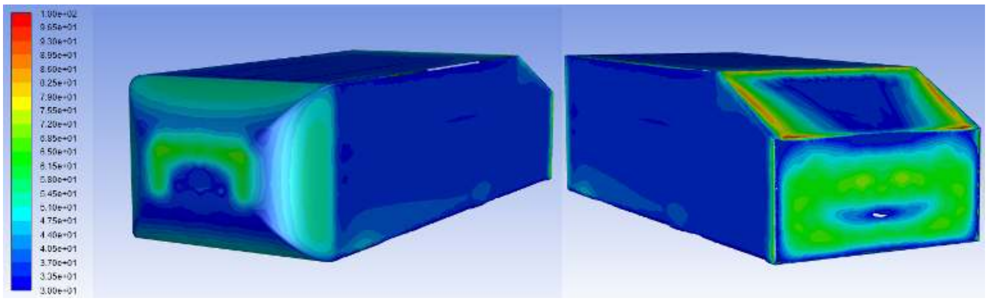

Figure 3.20. y+ monitor

The flow domain was similar to the wind tunnel. The total length of the area was 10 L and there was a distance of 2.4 L between the front of the model and the inlet. The width of the calculation area was twice the width of the model and the height was 1.5 L. To avoid the excessive distortion of the flow, the blockage ratio kept lower than 5%, as 4,61%. Since the model was symmetrical and the solution was a steady flow, the half body assumption was used.

In order to demonstrate the independence of the CFD solution from the number of mesh elements, analyses were performed with different element numbers. These element numbers was1.06, 2.12, 4.19 and 8.8 x 10^6, respectively. Considering that the result was not affected after the analysis with 4.19 x 10^6 element number, the remaining analyzes were completed around this element number.

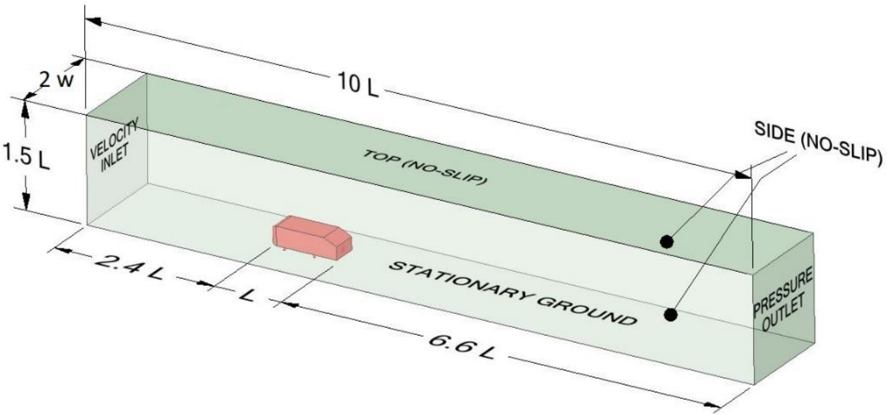

Figure 3.21. Flow domain

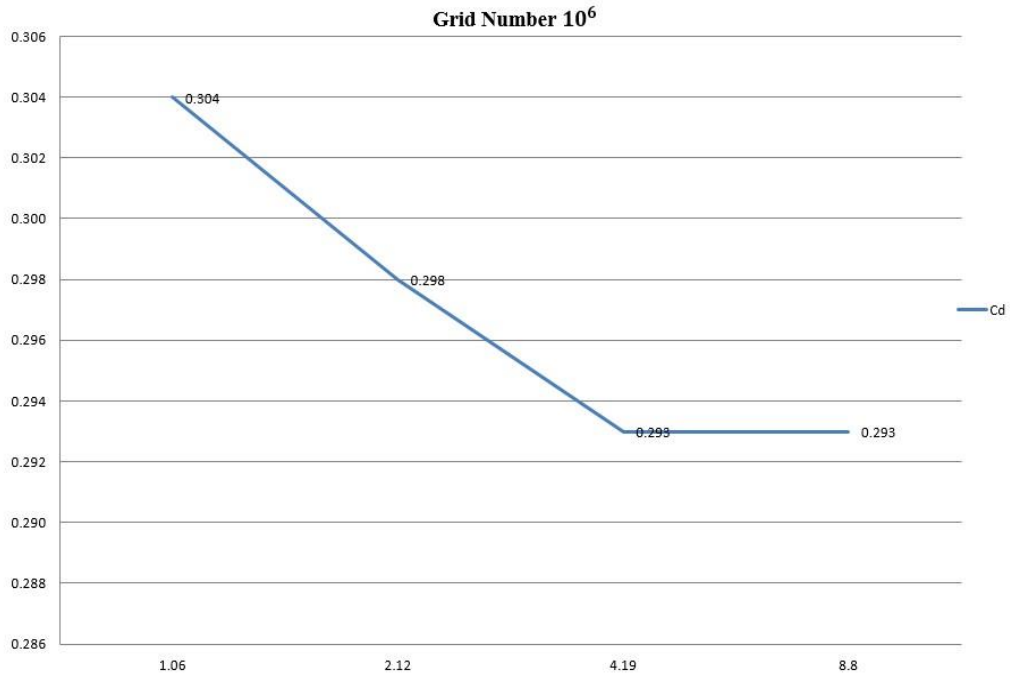

Figure 3.22. Mesh independency

3.3. Solving

The turbulence model is the model used to calculate the flow behaviour of the model in the determined flow domain. The choice of this model should be very important for an accurate calculation. To describe the flows of incompressible fluids in fluid mechanics, Navier-Stokes equation which is a partial differential equation has been developed. This equation is named after the French engineer and physicist Claude-Louis Navier and British physicist and mathematician Sir George Gabriel Stokes. Navier has introduced the element of viscosity (friction) for the more realistic and vastly more difficult problem of viscous fluids and Stokes improved this work. The incompressible Navier - Strokes Continuity equation can be writing as below,

Continuity: $$\frac{\partial \rho}{\partial t} + \frac{\partial (\rho u)}{\partial x} + \frac{\partial (\rho v)}{\partial y} + \frac{\partial (\rho w)}{\partial z} = 0$$

X-Momentum: $\frac{\partial(\rho u)}{\partial t} + \frac{\partial(\rho u^2)}{\partial x} + \frac{\partial(\rho uv)}{\partial y} + \frac{\partial(uw)}{\partial z} = - \frac{\partial \rho}{\partial x} + \frac{1}{Re_r}\left[\frac{\partial \tau_{xx}}{\partial x} + \frac{\partial \tau_{xy}}{\partial y} + \frac{\partial \tau_{xz}}{\partial z}\right]$

Y-Momentum: $\frac{\partial(\rho v)}{\partial t} + \frac{\partial(\rho uv)}{\partial x} + \frac{\partial(\rho v^2)}{\partial y} + \frac{\partial(pvw)}{\partial z} = - \frac{\partial \rho}{\partial y} + \frac{1}{Re_r}\left[\frac{\partial \tau_{xy}}{\partial x} + \frac{\partial \tau_{yy}}{\partial y} + \frac{\partial \tau_{yz}}{\partial z}\right]$

Z-Momentum: $\frac{\partial(\rho w)}{\partial t} + \frac{\partial(\rho uw)}{\partial x} + \frac{\partial(\rho vw)}{\partial y} + \frac{\partial(pw^2)}{\partial z} = - \frac{\partial \rho}{\partial z} + \frac{1}{Re_r}\left[\frac{\partial \tau_{xz}}{\partial x} + \frac{\partial \tau_{yz}}{\partial y} + \frac{\partial \tau_{zz}}{\partial z}\right]$

Based on this Navier - Stokes equation, Osborne Reynolds proposed the Reynolds - Averaged Navier - Stokes equation. Which is a time - averaged equation of motion for fluid flow. Thanks to Reynolds decomposition in this equation, instantaneous quantity is decomposed into its time-averaged and fluctuating quantities. RANS equations are principally used for the describe turbulent flows and one of the RANS based equation is, the k-ω SST turbulence model.

Throughout this study, the k-ω SST turbulence model was used, which had suitable properties for vehicle aerodynamics, as Raina et al., (2017) stated in their study. The model was first introduced by Menter, (1994). The model was a two-equation turbulence viscosity model based on Wilcox, (1988) k-ω SST model. k-ω SST is beneficial for estimating the viscous flow behaviour in the near-wall region and can, therefore, give accurate results when the adverse pressure gradient condition prevails. When it comes to far-field, flow behaviour shows a strong dependence on ω values even for non-turbulent flows, but this deficiency is not present in the k-ε model. To take advantage of this favourable feature of k-ε , Menter has combined the basic k-ω SST model with the k-ε model. This combination is done by writing the epsilon in the k-ε model of the transport equation under ω conditions. Thereby, k-ω SST preserves the favourable properties of 2 different turbulence models and becomes an accurate turbulence model. The SST turbulence model comprises two equations: one for k, the specific turbulent kinetic energy (m^2s^{-2}):

$$\frac{\partial}{\partial t}(\rho k) + \frac{\partial}{\partial x_i}(U_i \rho k) = \frac{\partial}{\partial x_j}\left(\mu_k \frac{\partial}{\partial x_j} k\right) + \tilde{P}_k - \beta^* \rho \omega k$$

And one for ω, the specific turbulent dissipation rate (or specific turbulent frequency) (s^{-1}):

$$\frac{\partial}{\partial t}(\rho\omega) + \frac{\partial}{\partial x_i}(U_i\rho\omega) = \frac{\partial}{\partial x_j}\left(\mu_\omega \frac{\partial}{\partial x_j}\omega\right) + P_\omega - \beta\rho\omega^2 + 2\rho(1 - F_1)\frac{1}{\omega}\frac{1}{\sigma_{\omega,2}}\frac{\partial}{\partial x_j}k\frac{\partial}{\partial x_j}\omega$$

This study carried out at the following parameters; pressure-based, steady-state incompressible turbulent flow at sea level under 15 °C air conditions. Ahmed et al., (1984), in their studies, there was a no inscription that the surface area of the stilts was added to the projected surface area of the model. In their study, Khan & Umale, (2014) did not add the surface area of the stilts to the projected surface area. Therefore, the stilts surface area were not added to the projected surface area and accepted as 0.112 m^2. As boundary conditions, the inlet set as velocity inlet, outlet set as pressure outlet, ground set as stationary ground, body and walls was set as stationary walls with no-slip conditions. At last, the symmetry plane was set as symmetry. Also, in velocity inlet, 'Turbulent Intensity' was set to 1% and 'Turbulent Viscosity Ratio' was set to 10. At the pressure outlet, 'Backflow Turbulent Intensity' was set to 5% and 'Backflow Turbulent Viscosity Ratio' was set to 10. The temperature of the air in the flow domain set as 15 ℃, density was 1.225 kg/m^3 and viscosity was equal to 1.7894 kg/-s^{-5}.

When starting the setup, the double-precision option was activated to get a more accurate result in the 'Fluent Launcher' dialogue box and the parallel process to reduce the solution time. As a solution method scheme coupled selected. The pressure-based coupled algorithm obtains a more robust and efficient single-phase implementation for steady-state flows. The least-squares cell-based scheme selected as a gradient. The least-squares cell-based gradient is less expensive to compute than the node-based gradient. Therefore, it is recommended that least-squares cell-based gradient reconstruction. Lastly, momentum, turbulent kinetic energy and specific dissipation rate options preferred as second-order upwind. For triangular and tetrahedral grids, since the flow was never aligned with the grid, generally second-order discretization gives more accurate results. In all of these analyses, convergency criteria were set as 10^{-4} for all parameters.

3.4. Validation

Since computational simulations have error percentage to real-life values, the error percentage must be as low as possible. Thus, an analysis has performed for the Ahmed body with 25° slanted surface, under the same experimental conditions (60 m/s, 4.2 x 10^6) that employed, Ahmed et al., (1984).

Result of this simulation was shown in Figure 3.23., together with experimental results provided in the experimental study used as a reference. As shown, the drag coefficient was almost predicted relatively to the experimental study. Concerning the drag coefficient, the difference from the experimental study was equal to 1.03%. However, unlike the fewer error margin of the drag coefficient compared to the experimental studies, the error margin of the lift coefficient can be around 16%.(Hughes, 2018)

Another parameter that can be used for validation was the pressure coefficient distribution on the top surface of the Ahmed body at the symmetry plane. From this point of view, Bayraktar et al., (2001) plotted experimental and numerical pressure coefficient values for various slant angles. Based on this comparison, the pressure coefficient distribution for both experimental and this base numerical study plotted in 3.24. Lastly, recirculation torus structure at the end of the Ahmed body was successfully achieved the same as Ahmed et al., (1984) stated. These two recirculation torus structure achieved from the numerical base study and presented by Ahmed et al. showed in Figure 3.25.

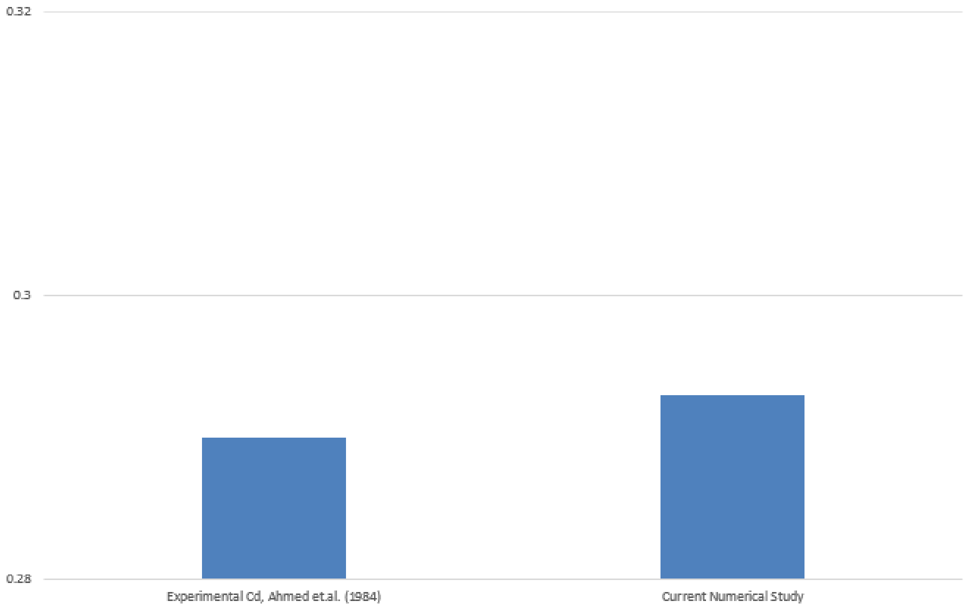

Figure 3.23. Difference between experimental and numerical (CFD) drag coefficient

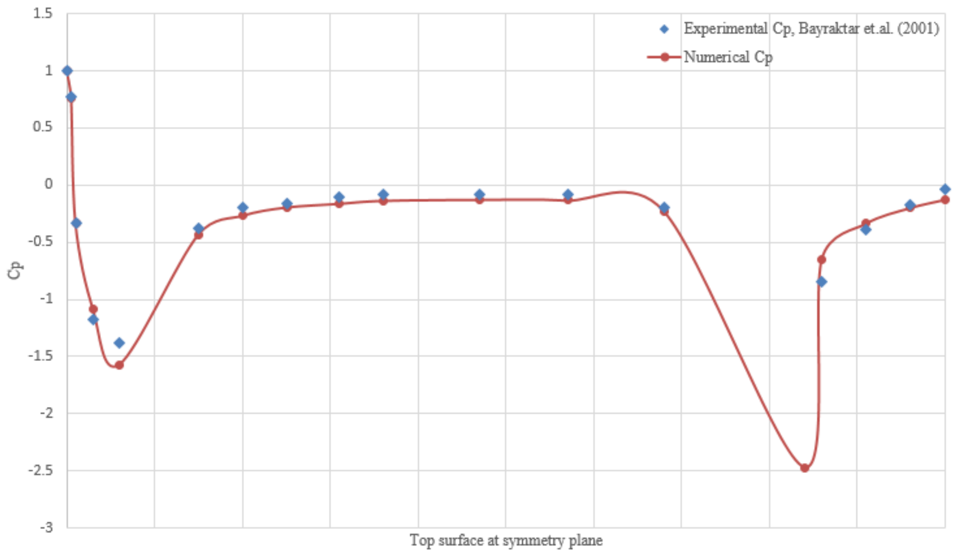

Figure 3.24. Pressure coefficient distribution on the top surface of Ahmed body, at the symmetry plane

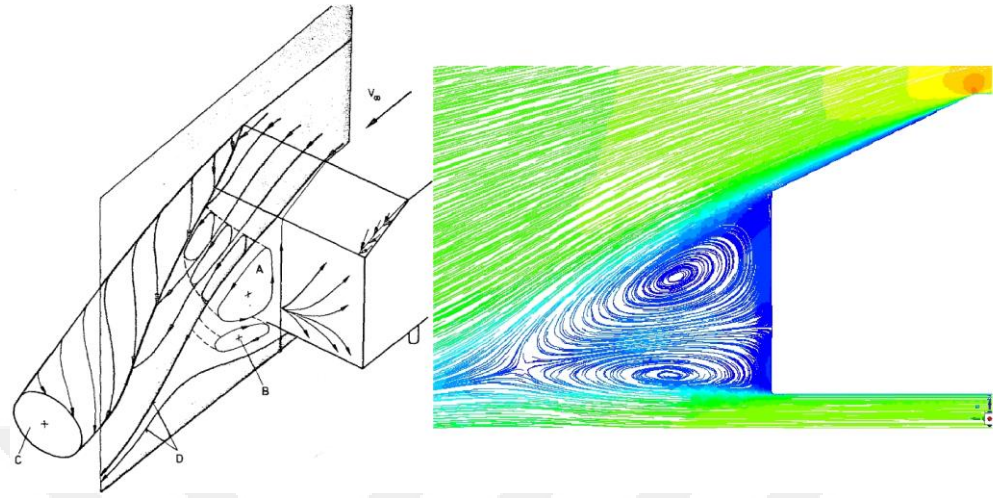

Figure 3.25. Recirculation torus at the rear end of Ahmed body, Left; Ahmed et al., (1984) Right; current numerical study

4. RESULTS

The results were divided into 5 sections. In the first 4 sections, the results of the 'Curvature', 'Deflector', 'Optimum' and 'Relocated Deflector' control methods were displayed. At the last section detail examination of the best-resulted control models were presented. In 'Curvature' and 'Deflector' control methods, each control model was compared between them and the uncontrolled model. After comparing all the models in these control methods based on 'C_d' and 'C_l' parameters among themselves, detailed examinations of the models with the best results were presented. After defining the models that give the best 'C_d' result in these 2 control methods, these models were used in 'Relocated Deflector' and 'Optimum' control methods. All these analyses were solved in as same conditions as mentioned in the previous section. Results are based on converged solutions.

To better understand the effects of these control methods on drag and lift coefficients, the analysis called 'Uncontrolled' executed. In this analysis, Ahmed Body keeps as the original. As a result of this analysis, for C_d = 0.293 and C_l = 0.391 received. To maintain a better comparison between oncoming control methods and original flow structures, parameters for the 'Uncontrolled' case also presented below (will be named as ‘base’ in parameter comparison).

4.1. Curvature Control Method

The first control method, the influence of the curvature applied on the upper edge of the slanted surface was examined. As a mentioned previous chapter, curvature radius differed from 200 to 1000 mm. After carrying out analyses, drag and lift coefficients are obtained and results were compared within themselves and uncontrolled case. Results are shown below in Figure 4.1. and Figure 4.2.

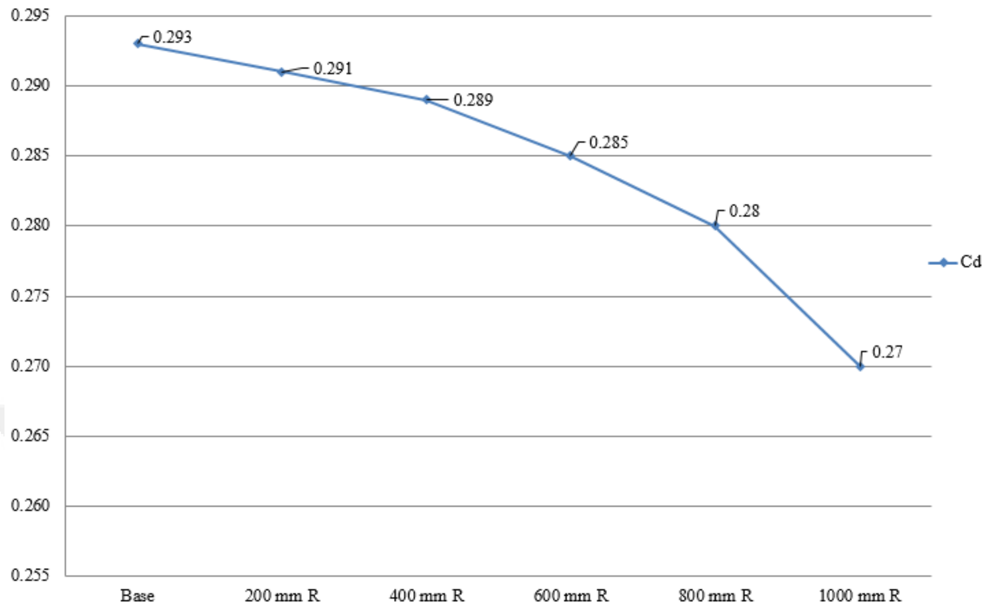

Figure 4.1. Drag coefficients of Curvature Control method

It can be seen clearly from the results, as the curvature radius increase drag coefficient decreasing. When the curvature radius was 1000 mm, the drag coefficient gives the lowest value.

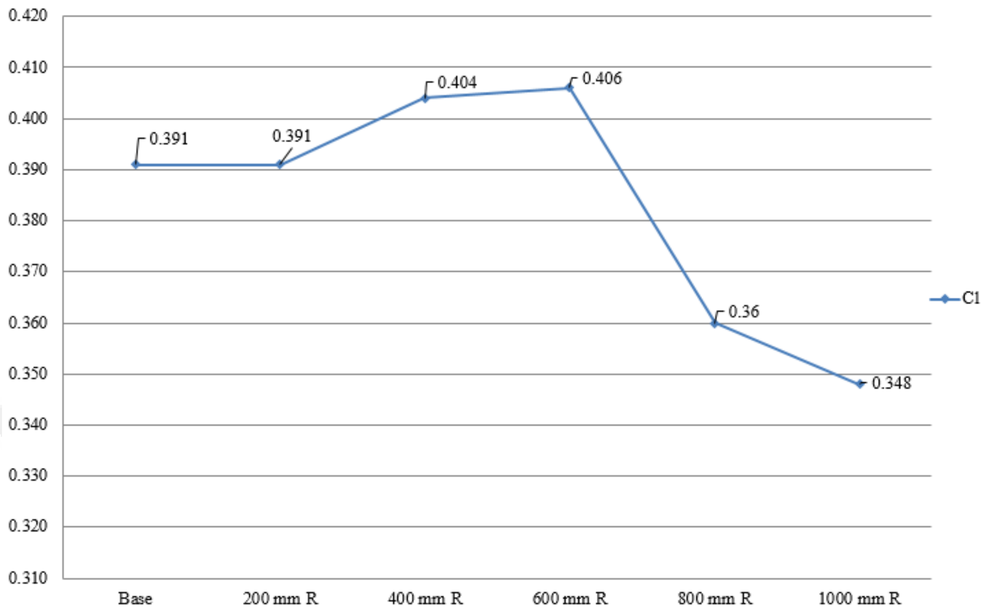

Figure 4.2. Lift coefficients of Curvature Control method

Nevertheless, the lift coefficient remains the same as the uncontrolled case at 200 mm curvature radius. For the 400 and 600 mm radius models, the lift coefficient tends to increase. After exceeding 600 mm curvature radius, the lift coefficient decrease dramatically.

By taking into consideration to results, the best-given result for curvature control method was 1000 Radius model. For this reason, the flow examined more detailed for 1000 radius applied curvature control. Thus, various parameters were presenting. These parameters were the same as the given in Uncontrolled Case above (will be named as ‘1000R’ in parameter comparison).

4.2. Deflector Control Method

In this control method, the influence of the deflector on the lower edge of the slanted surface was investigated. As mentioned previous, deflector length differs from 1% to 6%of the model length. After carrying out analyses, drag and lift coefficients are obtained and results were compared within themselves and uncontrolled case. Results are shown below in Figure 4.3. and Figure 4.4.

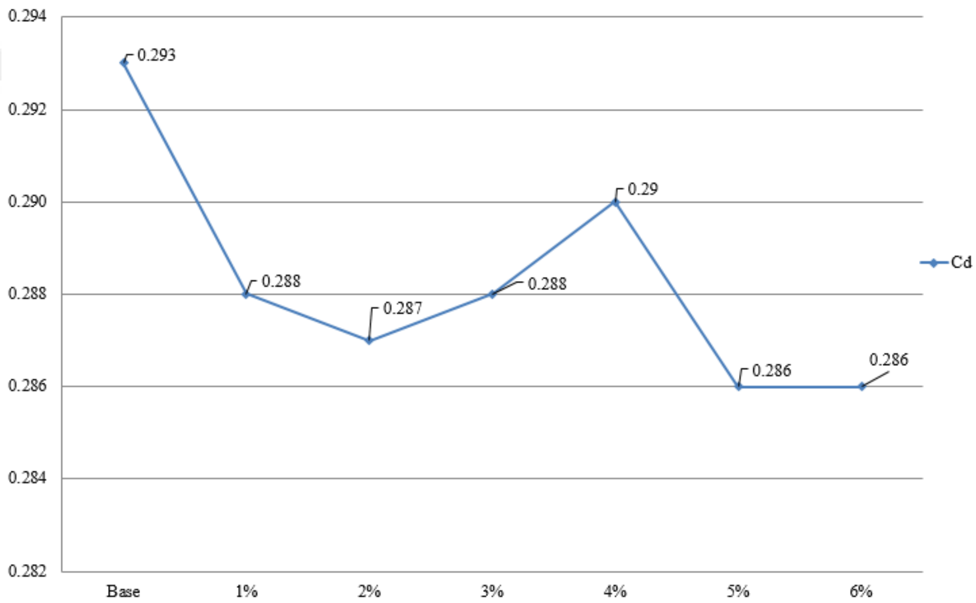

Figure 4.3. Drag coefficients of Deflector Control method

As the analyses results indicate us, there was a no correlation between the deflector length and the drag coefficient. For the 1 and 3%, deflector model results were the same, also result of the 2% deflector model was almost the same as these models. The 4% deflector length model, which was among the control method models, gave the worst result for this control method. However, after the length exceeded 4% of the model length, the drag coefficient decreased. Thus, the best drag coefficient results achieved with 5% and 6% deflector length models.

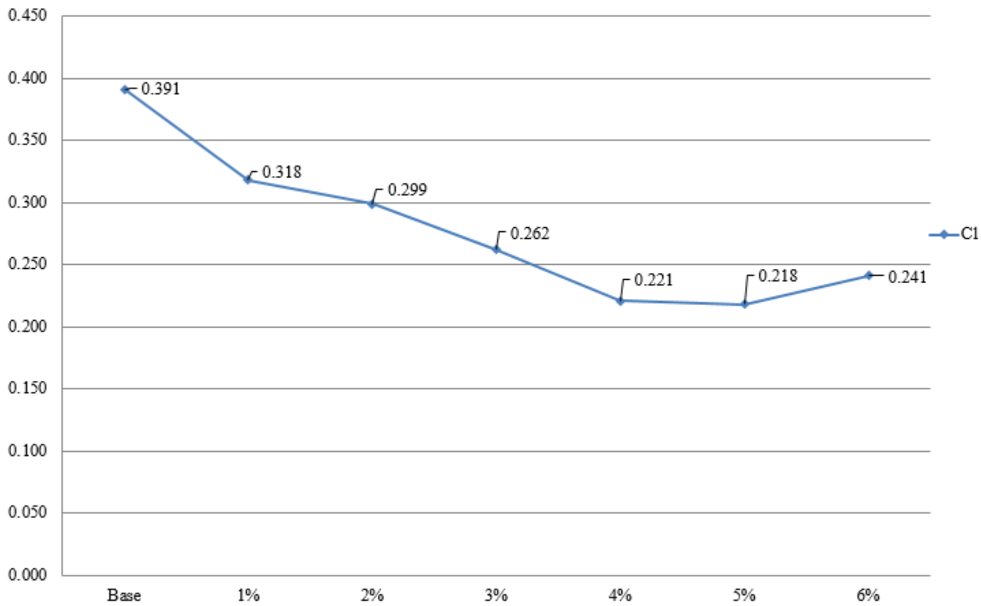

Figure 4.4. Lift coefficients of Deflector Control method

In other respects, the lift coefficient indicates correlations between deflector length and lift coefficient decrease until the deflector length was equal to 5% of the body length. In the deflector model with 6% deflector length, the lift coefficient was slightly increased.

By taking into consideration to deflector control method results, the best-given results were 5 and 6% deflector length models. Since the 5 and 6% deflector length were given the same drag coefficient, a prestudy was made to decide between these two lengths and as a result of this prestudy 6%, deflector length was used in this control method. Following parameters shown below (will be named as ‘d6’ in parameter comparison).

4.3. Optimum Control Method

In this control method, the best model results from the first two control methods were merged. 1000 mm curvature radius applied to the upper edge and located the 6% deflector length to the lower of the slanted surface. After the analyse this optimum control method, the results were compared with the uncontrolled, 1000 mm curvature radius applied and the 6% deflector length attached model.

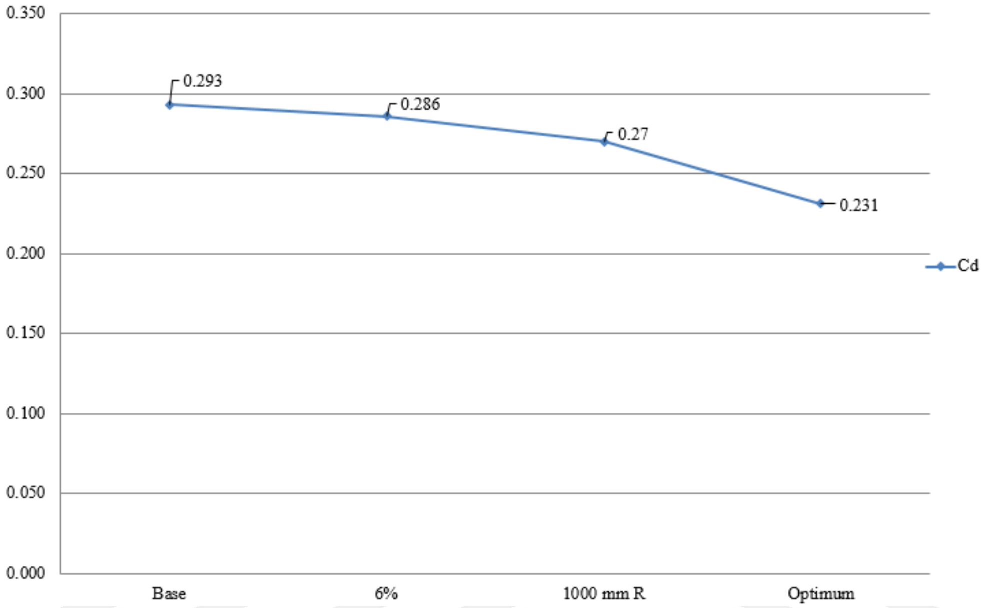

Figure 4.5. Drag coefficients of Optimum Control method

As you can see in the above, thanks to merging of the first two models, the drag coefficient becomes lower than these models.

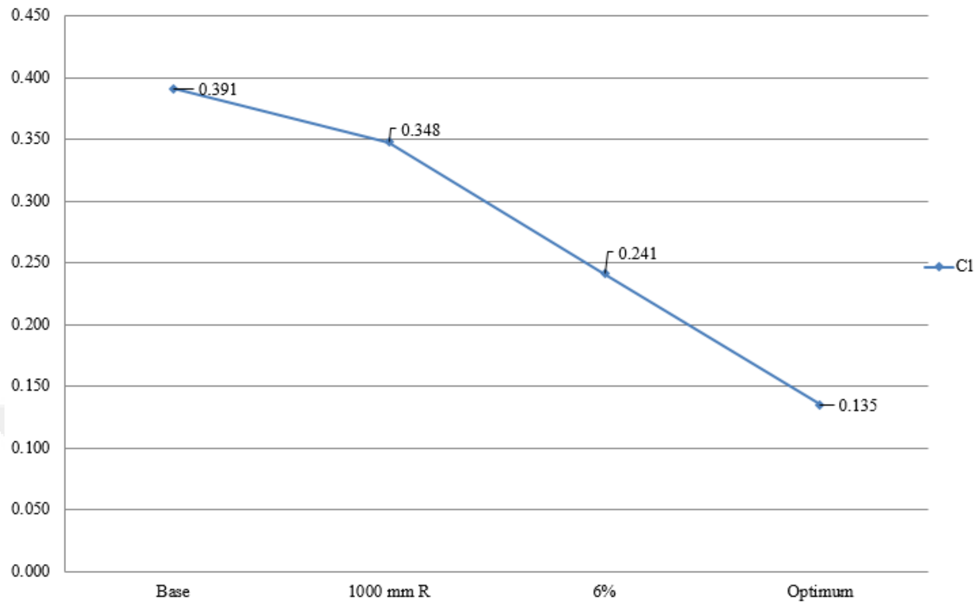

Figure 4.6. Lift coefficients of Optimum Control method

As the same as in the drag coefficient, also the lift coefficient shows a similar trend. Optimum control method model gives better results than curvature and deflector control models. To better examine the flow, parameters are given below (will be named as ‘op6’ in parameter comparison).

4.4. Relocated Deflector Control Method

As mentioned in the previous section, there are dimensional limits that the models have to comply with. Based on this fact, the 6% long deflector was repositioned on the slanted surface, which was the best-given drag coefficient result. To figure out effects to drag and lift coefficients this relocated deflector model, results were compared with uncontrolled and 6% deflector length analyses results. Results are shown below.

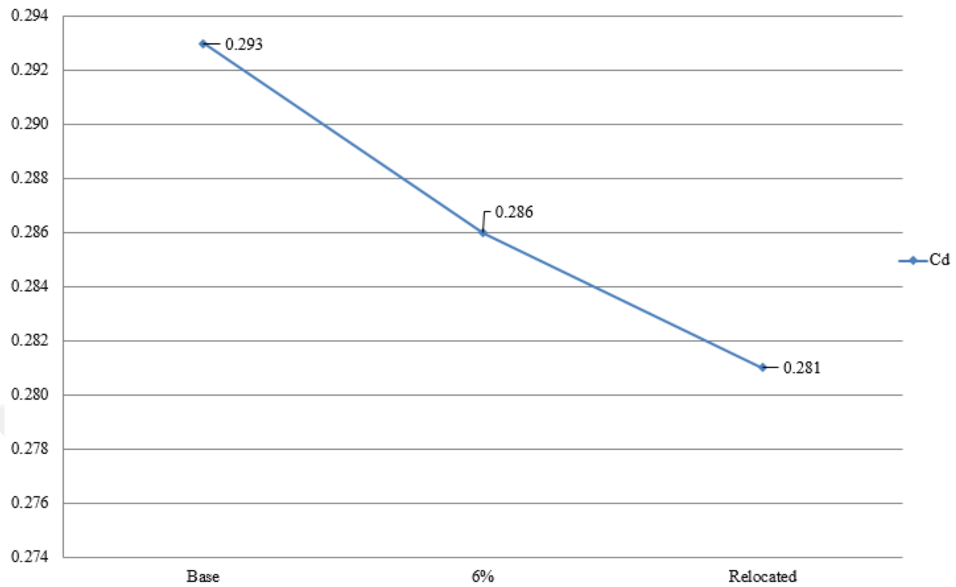

Figure 4.7. Drag coefficients of Relocated Deflector Control method

As the result indicates us, thanks to the relocation of deflector on the slanted surface drag coefficient was lower than the lower edge of the slanted surface located deflector.

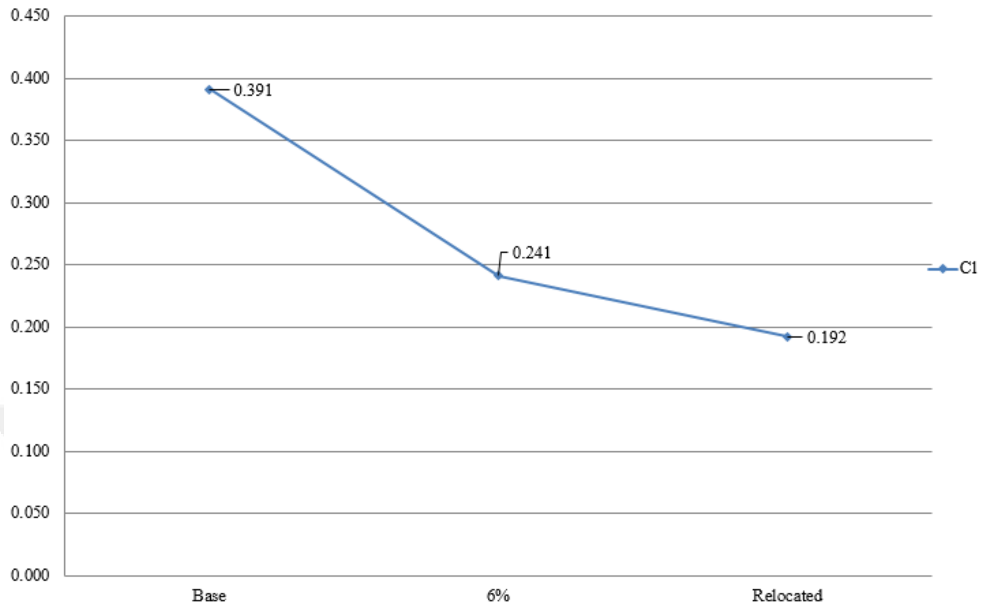

Figure 4.8. Lift coefficients of Relocated Deflector Control method

In addition, the lift coefficient gave a better result than the previous method. To better examine the flow, parameters are given below (will be named as 'rl6' in parameter comparison).

4.5. Detailed Examination

In this chapter, the best results achieved from the analyses compared according to their Static and Total Pressure, Turbulent Kinetic Energy, Velocity and Vorticity. As mentioned earlier, 'Uncontrolled' simulation named as 'base', 1000 mm radius applied curvature control named as '1000R', deflector control method named as 'd6', optimum control method named as 'op6' and finally relocated deflector control method named as 'rl6'.

The first plane used in detailed examinations was 'Symmetry' plane. From this Symmetry plane, 'Static and Total Pressure', 'Turbulent Kinetic Energy', 'Velocity' and 'Vorticity' parameters presented. Furthermore, 'Total Pressure' and 'Velocity' parameters presented from 'Top' called a plane, at z/l=0.23 (which is the same height as end of the slanted surface z = 244 mm). Finally, 'Total Pressure' and ‘Velocity Magnitude’ from the plane called 'End' at y/ *l* =0.21 (which is 0.220 mm behind the rear end of the model). This downstream transversal plane, the location was already used in (Fourrié et al., 2011) for the comparison.

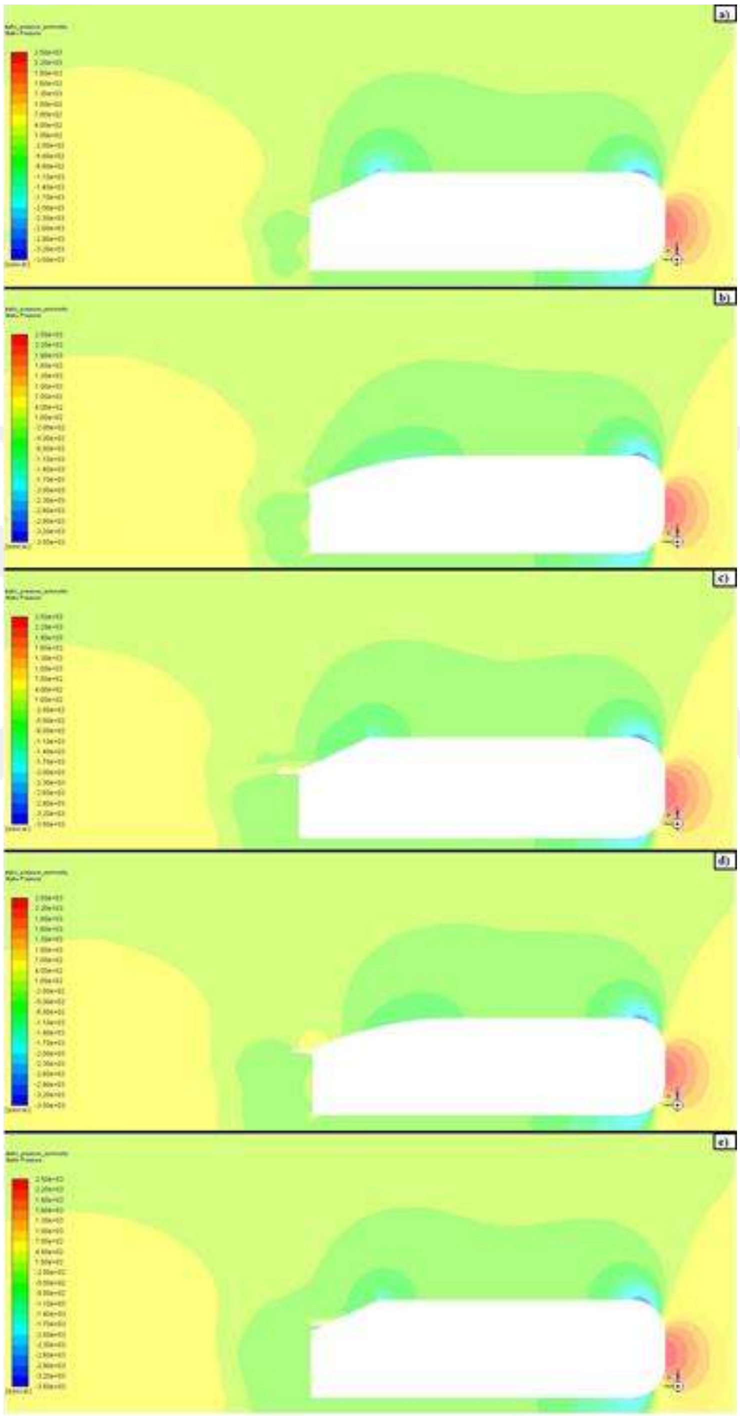

Figure 4.9. Static Pressure on symmetry plane, a)base, b)1000R, c)d6, d)op6, e)rl6

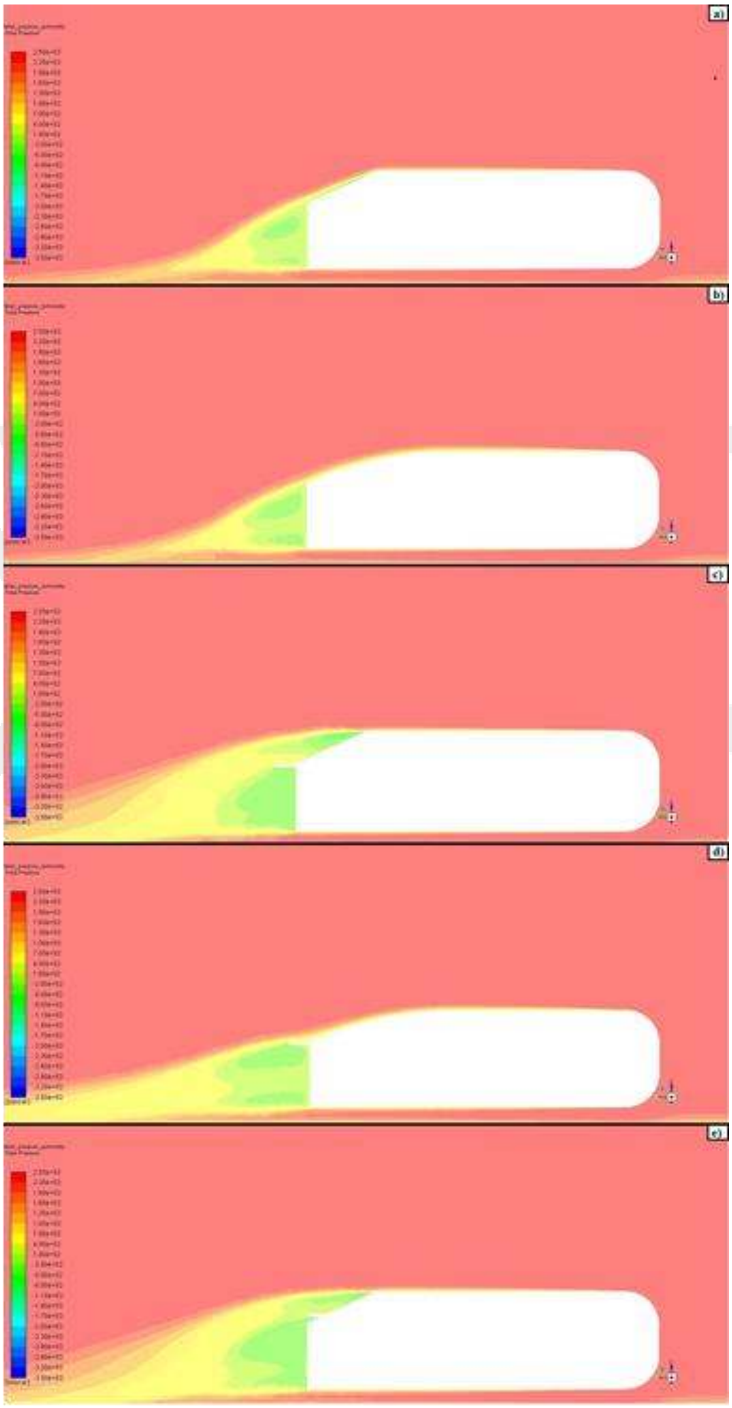

Figure 4.10. Total Pressure on symmetry plane, a)base, b)1000R, c)d6, d)op6, e)rl6

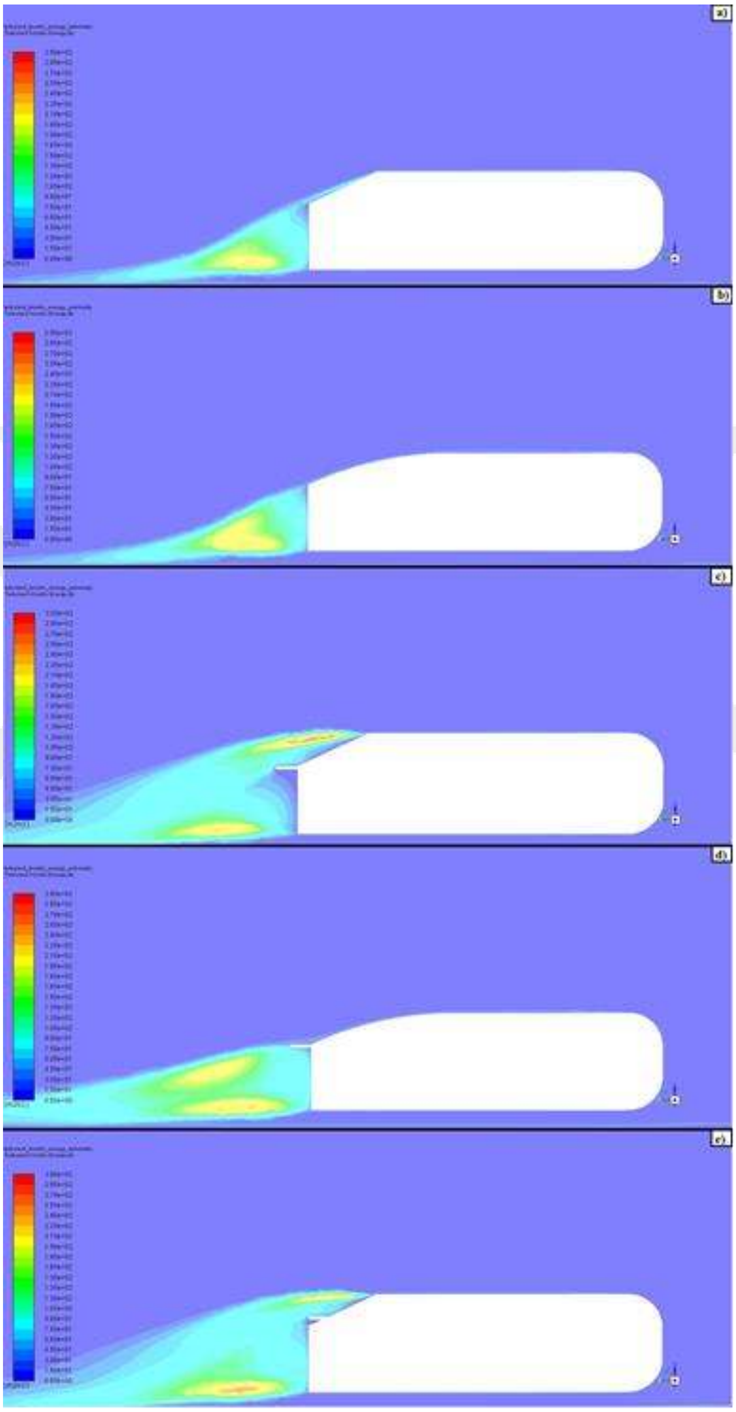

Figure 4.11. TKE on symmetry plane, a)base, b)1000R, c)d6, d)op6, e)rl6

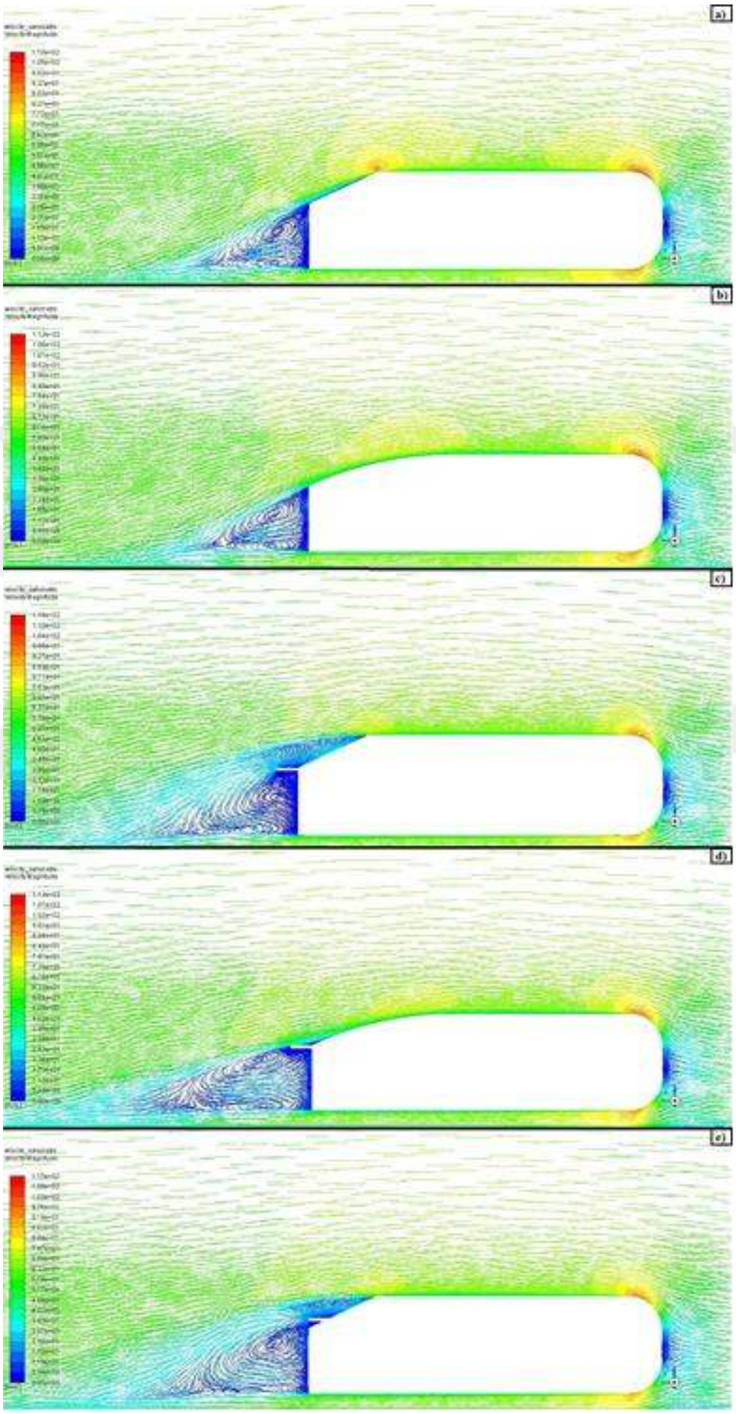

Figure 4.12. Velocity on symmetry plane, a)base, b)1000R, c)d6, d)op6, e)rl6

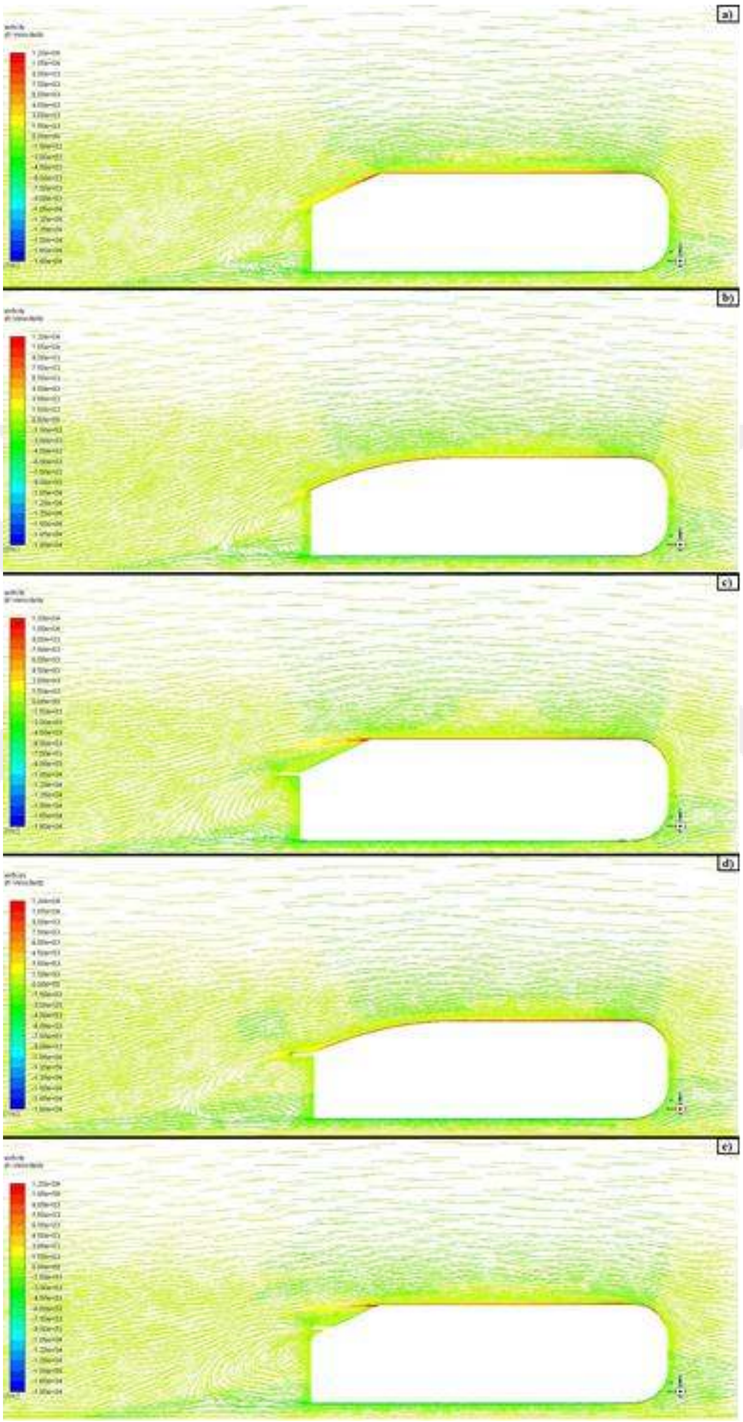

Figure 4.13. Vorticity on symmetry plane, a)base, b)1000R, c)d6, d)op6, e)rl6

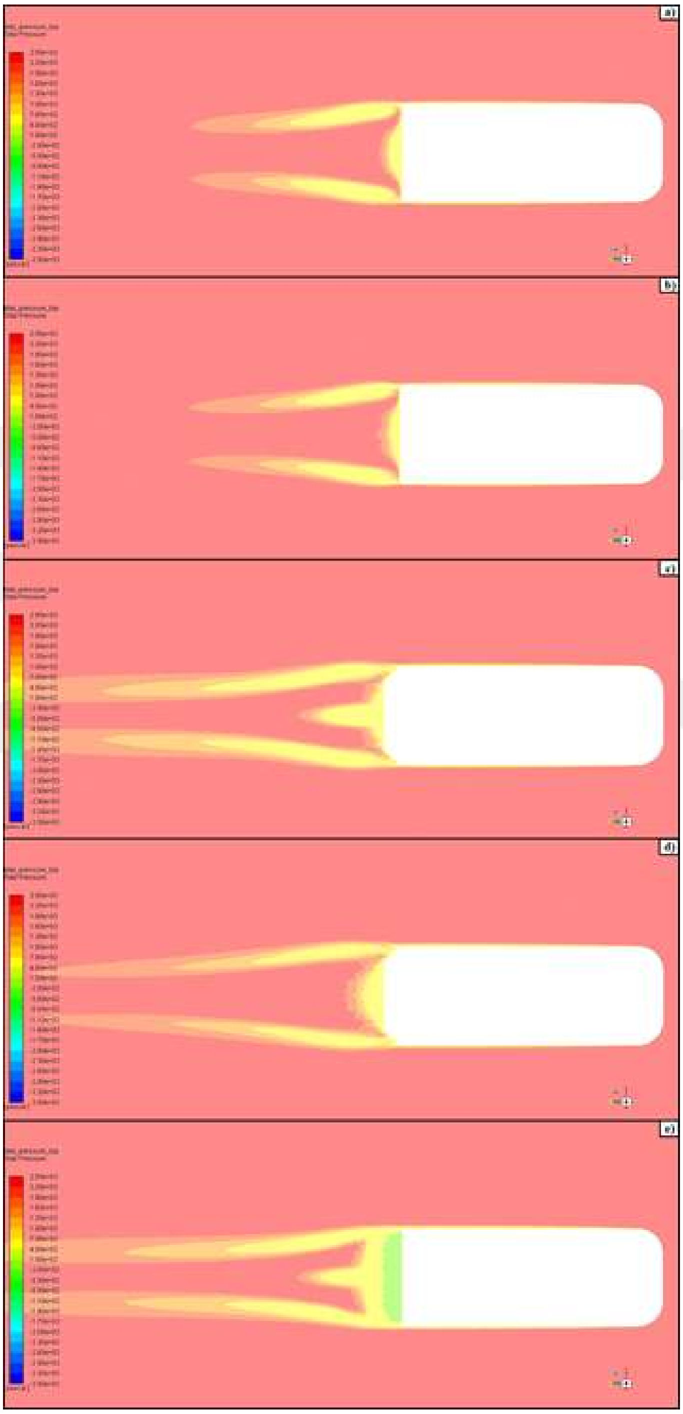

Figure 4.14. Total Pressure on z/*l*=0.23, a)base, b)1000R, c)d6, d)op6, e)rl6

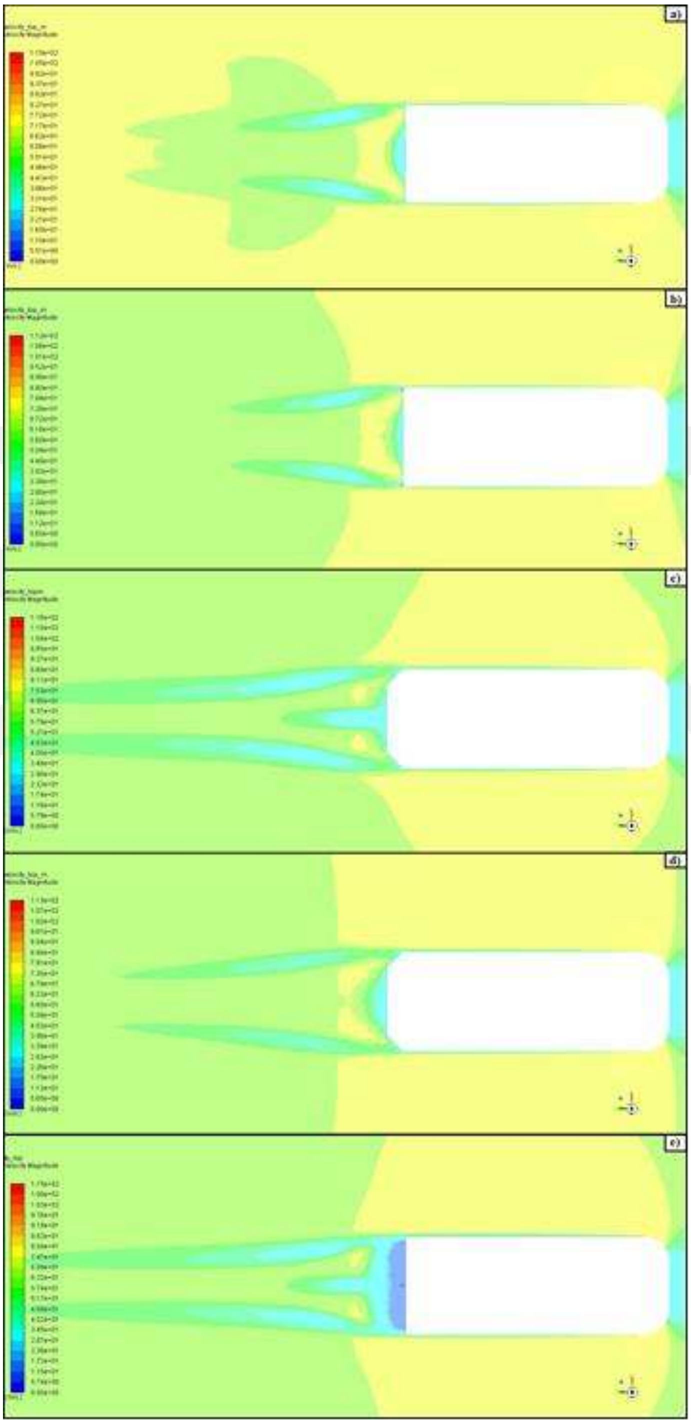

Figure 4.15. Velocity Magnitude on z/*l*=0.23, a)base, b)1000R, c)d6, d)op6, e)rl6

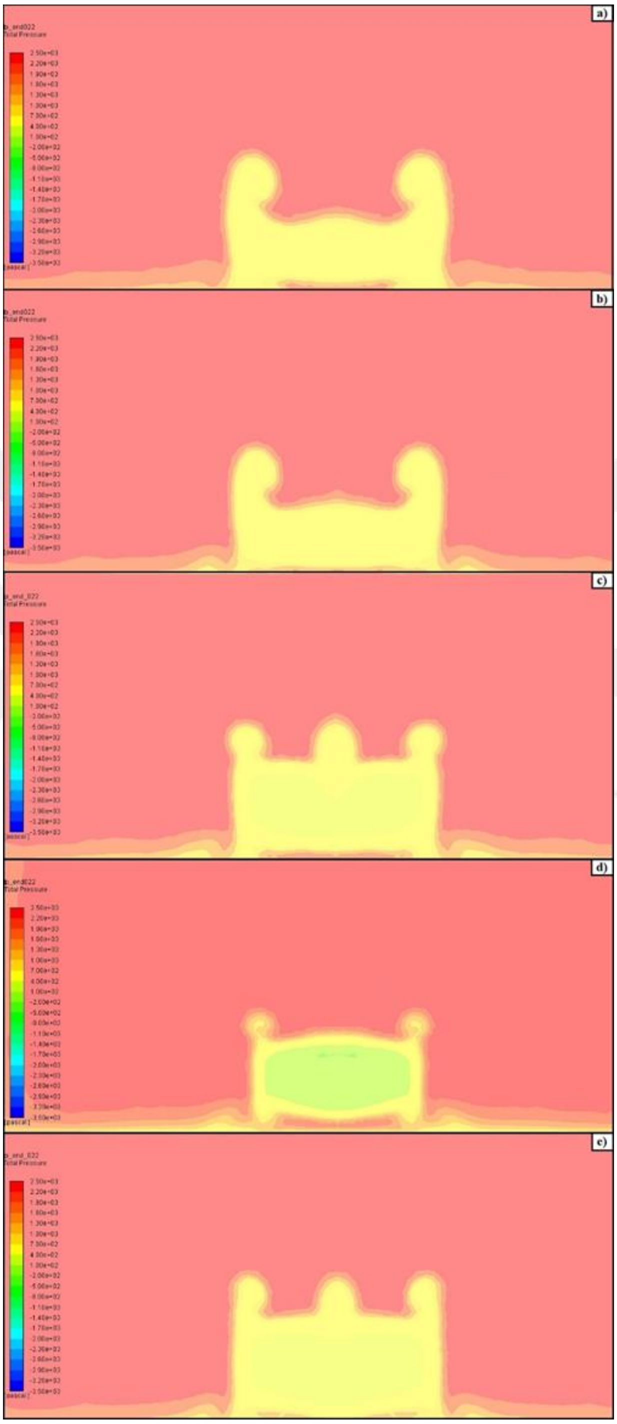

Figure 4.16. Total Pressure on y/ l =0.21, a)base, b)1000R, c)d6, d)op6, e)rl6

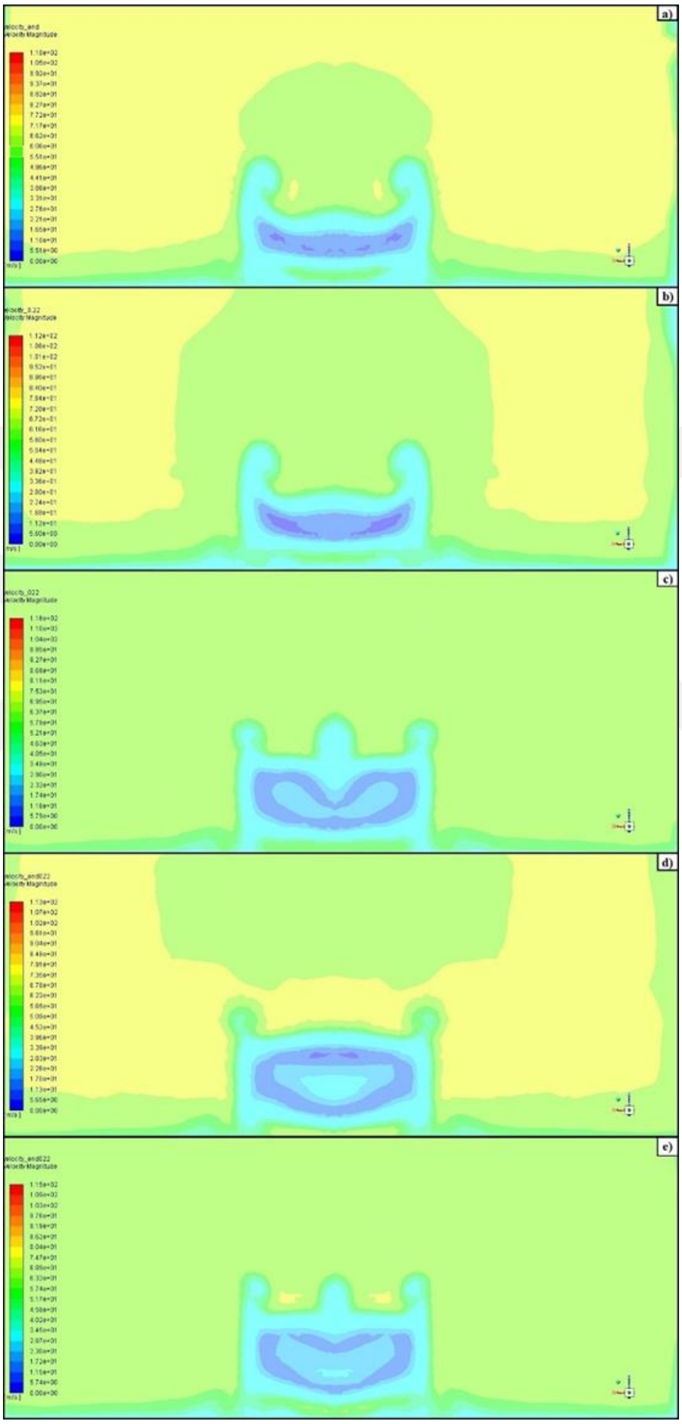

Figure 4.17. Velocity Magnitude y/ l =0.21, a)base, b)1000R, c)d6, d)op6, e)rl6

4.5.1. Drag and Lift Coefficient

As you can see above, the drag and lift coefficients obtained from controlled body simulations are shown in **Figures 4.1. - 4.2**.

In the curvature control method, drag coefficient decreases dramatically when the applied curvature reaches the 1000 radius. Moreover, the lift coefficient was dramatically reduced after the 600 mm radius applied curvature control model with the highest result. This decrease in the drag coefficient was due to the absence of the separation bubble in the slanted surface. Moreover, the absence of low static pressure core on the upper side of the slanted surface creates a fully attached flow in this region.

In the deflector control method, drag and lift coefficient also decrease, but this decreasing was not as much as the curvature control method. In this control method, the separation bubble continues to occur on the slanted surface and the low-pressure zone in the upper side of the slanted surface was almost the same as base simulation. The main reason for drag and lift coefficients reduction was the disordered recirculation torus in the rear end of the model.

As a third control method, the optimum control method was given the best result in terms of both drag and lift coefficient. As explained above, the optimum control method showed the positive contributions of both control methods on which it was based. There was a no separation bubble in this control model as in the 1000R control model. In addition, thanks to the deflector, recirculation torus structures at the rear end of the model have moved away from each other and from the end of the model, as can be seen on the 'Turbulent Kinetic Energy', 'Total Pressure' and 'Velocity' monitors.

Finally, a considerable reduction in drag coefficient was not achieved in the relocated deflector control method. While the separation bubble structure was partially disseminated with the deflector placed on the slanted surface, the lower recirculation torus at the end of the model has become a more powerful structure, as can be seen on the 'Turbulent Kinetic Energy' monitor.

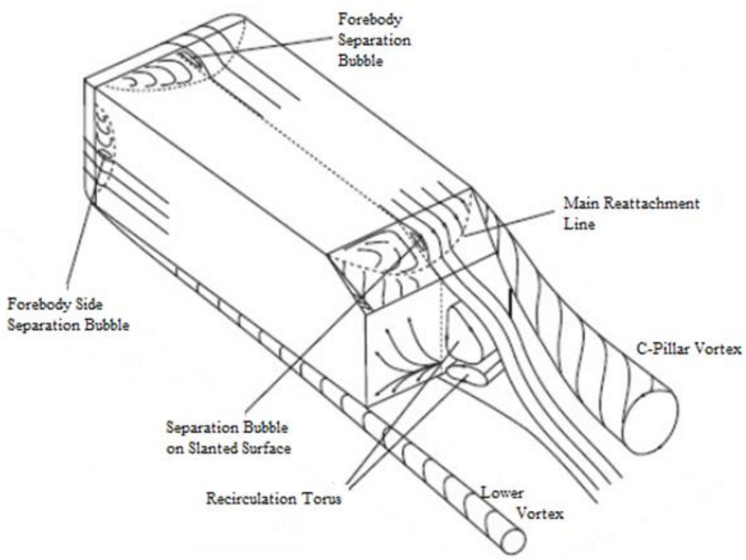

Figure 4.18. Flow structures around Ahmed Body

4.5.2. Wake Zone

As mentioned earlier, aerodynamic drag mainly caused by the pressure difference between the front and back of the Ahmed body. In this chapter, the rear wake of the models explained more detailed.

According to the 'End' (**y/ *l* = 0.21**) plane and predicated on the base model, it can be seen the smallest c-pillar vortices in the op6 model. After that, the rl6 control model has the mid-sized c-pillar vortices and when it comes to the d6 control model the c-pillar vortices almost remains the same with the base model. From here, it can be understood that as the diameter of the c-pillar vortices decreases, it contributes to the drag reduction positively.

As seen from the 'Top' (**z/*l* = 0.23**) plane thanks to the total pressure monitor, it can be seen the c-pillar vortices length on each control model. Again predicate on the base model, on the 1000R control model c-pillar vortices length was almost the same as the base model but the diameter of these vortices slightly smaller than the base model. On the d6 and rl6 control models, the length of the c-pillar vortices was almost twice the length of the base model and the length of the op6 control models c-pillar vortices was slightly shorter than these two control method. Nevertheless, the diameter of the op6 c-pillar vortices was smaller and slightly far from the centre than other control models c-pillar vortices. Considering the simulation results, it can be seen as the diameter of c-pillar vortices decreases, the coefficient of drag decreases. Results clearly show there was a no correlation between the length of the c-pillar vortices and the drag coefficient.

Another thing that differs in the model wake was the structure of the delayed separation bubble. In the base model wake, the separation bubble was reattaching to the slanted surface but for the d6 and rl6 control models, the separation bubble does not reattach on the slanted surface. Thus, the delayed separation bubble structure occurs. This delayed separation bubble in the wake was the largest for d6 control model, for both drag and lift coefficient result indicate us there was a no correlation between the growing delayed separation bubble structure and drag nor lift coefficient.

Lastly, because of there was a no characteristic recirculation torus structure in d6 and rl6 control models also the absence of delayed separation bubble structure in 1000R and op6 control models, the explanation of the best-resulting control model op6, was made by recirculation torus comparison. As you can see in the symmetry plane turbulent kinetic energy monitor, there was a strong lower recirculation torus bonded with upper recirculation torus in the base model. As for the 1000R control model, the upper and lower recirculation torus keep bonded but this time size of these two structures was almost equal with each other and results indicate us the drag and lift coefficients was decreasing. For the op6 control model, the size of the upper and lower recirculation torus remained almost equal-sized, but they moved away from the model end and each other. So, this shows us if the sizes of the upper and lower recirculation torus were equal and they were far from the end of the model, drag and lift coefficients tended to decrease.

5. CONCLUSION

The aim of this study was obtaining a drag reduction on the Ahmed body through passive control methods. Control methods were based on a 25° slant angled Ahmed body, first of this control method was curvature applied upper edge of the slanted surface and the second one was deflector attached to the lower edge of the slanted surface. Both for the radius of curvature and length of the deflector increased systematically. Beside these control methods, a new optimum control method was generated from the best-given results of curvature and deflector control methods. First of these control methods was merging curvature applied upper edge of the slanted surface and deflector attached to the lower edge. Secondly, best-given deflector control method length has been used for relocation the deflector on the slanted surface.

Investigations were conducted under the same 60 m/s inlet velocity (Reynolds = 4.2×10^6) condition, k-ω SST turbulence model was used to resolve numerically the flow around base and control models.

The static and total pressure, turbulent kinetic energy, velocity and vorticity monitors displayed on the symmetry plane. To better understand wake structures also total pressure and velocity magnitude monitors displayed from **z/l = 0.23** and **y/l = 0.21** planes. Through these selected monitors, flow features around the models were well predicted, such as the c-pillar vortices also known as longitudinal vortices, separation bubble and recirculation torus. The main conclusions of this study were summarized below.

Curvature applied at the upper edge of the slanted surface leads to the drag coefficient reduction. For the 1000 mm radius applied curvature control (1000R), the coefficient of drag was 7.84% reduced compared to the base model. Either the coefficient of lift reduced by 10.99% compared to the base model. Since the size of the separation bubble correlated positively to the drag coefficient, the absence of this structure leads to the drag reduction. Thanks to the 1000R control model's rounded upper edge flow over the model always remain attached to the slanted surface.

Deflector attached at the lower edge of the slanted surface lead to the drag reduction. Compared to the curvature applied control model, the coefficient of drag reduction was low. Both for the 5% and 6% deflector lengths coefficient of drag reduction was the same 2.38%. Nevertheless, for the lift coefficient, the deflector control method was more effective than curvature applied control model. Thanks to the 5% and 6% deflector lengths the lift coefficients were reduced by 44.24% and 38.36%. In the deflector control model, the separation bubble does not reattach to the slanted surface. As in the displayed in the previous chapter, because of the delayed separation bubble structure, the pressure on the slanted surface relatively lower. Also, the upper recirculation torus disappears from the end of the model. This two phenomenon effect on the drag coefficient quite minor but relatively major to the lift coefficient.

The optimum control model was the merge of the curvature and deflector control models. Its clearly seen 1000 curvature radius more effective than other curvature radiuses by far. However, when it comes to the deflector length it seems to 5% deflector length more suitable according to the results. Since its known, as the recirculation torus structure moves away from the end of the model, the coefficient of drag decreases. Thus, a prestudy was conducted to decide the deflector length for optimum control model. In this prestudy, 1000 mm radius applied and deflectors with two different lengths (5 and 6%) were attached on the lower edge of the slanted surface. As a result, 6% deflector length was more effective than 5% deflector length. Thus, both for optimum and relocated control models, 6% deflector length was used. As a result of combining 1000 mm curvature radius and 6% deflector length, the coefficient of drag and lift much lower than base control models. Coefficient of drag was reduced by 21.16% compared to the base model. For the coefficient of lift, the reduction was 65.47% compared to the base model. As stated earlier, thanks to curvature applied upper edge, there was a no separation bubble exist on the slanted surface. Besides this advantage, thanks to the deflector, recirculation torus structure moved away from the end of the model. Also, upper and lower recirculation torus moved away from each other. Combination of these two phenomena a major reduction obtained both for drag and lift coefficients.

Lastly, 6% deflector length was relocated on the slanted surface, to obtain drag and lift coefficient reduction without exceeding Ahmed body's dimensions. For this end of the deflector was aligned vertically with the end of the Ahmed body. As a result of this control method, the coefficient of drag was reduced by 4.09%. For the lift coefficient reduction was 50.89%. This control model’s results were better than the deflector attached lower edge. This more effective reduction was coming from a more powerful lower recirculation torus than the deflector control model. Also, since relocated deflector spoils the flow on the slanted surface, the size of the delayed separation bubble was lower than the deflector control model.

REFERENCES

Ahmed, S. R., Ramm, G., & Faltin, G. (1984). *Some Salient Features Of The Time-Averaged Ground Vehicle Wake*.

Altaf, A., Omar, A. A., & Asrar, W. (2014). Passive drag reduction of square back road vehicles. *Journal of Wind Engineering and Industrial Aerodynamics*, *134*, 30–43.

Bayraktar, I. (2002). External aerodynamics of heavy ground vehicles: Computations and wind tunnel testing. *ProQuest Dissertations and Theses*, 114.

Bayraktar, I., Landman, D., & Baysal, O. (2001). Experimental and computational investigation of Ahmed body for ground vehicle aerodynamics. *SAE Technical Papers*, *724*.

Beaudoin, J. F., Cadot, O., Aider, J. L., Gosse, K., Paranthoën, P., Hamelin, B., Tissier, M., Allano, D., Mutabazi, I., Gonzales, M., & Wesfreid, J. E. (2004). Cavitation as a complementary tool for automotive aerodynamics. *Experiments in Fluids*, *37*(5), 763–768.

Beaudoin, Jean François, & Aider, J. L. (2008). Drag and lift reduction of a 3D bluff body using flaps. *Experiments in Fluids*, *44*(4), 491–501.

Fourrié, G., Keirsbulck, L., Labraga, L., & Gilliéron, P. (2011). Bluff-body drag reduction using a deflector. *Experiments in Fluids*, *50*(2), 385–395.

Guilmineau, E. (2008). Computational study of flow around a simplified car body. *Journal of Wind Engineering and Industrial Aerodynamics*, *96*(6–7), 1207–1217.

Ha, J., JEONG, S., & OBAYASHI, S. (2011). DRAG REDUCTION OF A PICKUP TRUCK BY A REAR DOWNWARD FLAP. *International Journal of …*, *12*.

Hanfeng, W., Yu, Z., Chao, Z., & Xuhui, H. (2016). Aerodynamic drag reduction of an Ahmed body based on deflectors. *Journal of Wind Engineering and*

Industrial Aerodynamics, *148*, 34–44.

Hucho, W. H., & Sovran, G. (1993). *Aerodynamics of road vehicles*. 485–537.

Hughes, T. (2018). *CFD Study of Flow over a Simplified Car (Ahmed Body) Using Different Turbulence Models*. *June*, 0–47.

Huminic, A. and H. G. (2017). AERODYNAMIC STUDY OF A GENERIC CAR MODEL WITH WHEELS AND UNDERBODY DIFFUSER. *International Journal of ...*, *18*.

Khan, R. S., & Umale, S. (2014). CFD Aerodynamic Analysis of Ahmed Body. *International Journal of Engineering Trends and Technology*, *18*(7), 301–308.

Le Good, G. M., & Garry, K. P. (2004). On the use of reference models in automotive aerodynamics. *SAE Technical Papers*, *2004*(724).

Menter, F. R. (1994). Two-equation eddy-viscosity turbulence models for engineering applications. *AIAA Journal*, *32*(8), 1598–1605.

Morel, T. (1978). Aerodynamic drag of bluff body shapes characteristic of hatch-back cars. *SAE Technical Papers*, 1270–1279.

Pujals, G., Depardon, S., & Cossu, C. (2010). Drag reduction of a 3D bluff body using coherent streamwise streaks. *Experiments in Fluids*, *49*(5), 1085–1094.

Raina, A., Harmain, G. A., & Haq, M. I. U. (2017). Numerical investigation of flow around a 3D bluff body using deflector plate. *International Journal of Mechanical Sciences*, *131–132*(June), 701–711.

Strachan, R. K., Knowles, K., & Lawson, N. J. (2007). The vortex structure behind an Ahmed reference model in the presence of a moving ground plane. *Experiments in Fluids*, *42*(5), 659–669.

Thacker, A., Aubrun, S., Leroy, A., & Devinant, P. (2012). Effects of suppressing the 3D separation on the rear slant on the flow structures around an Ahmed body. *Journal of Wind Engineering and Industrial Aerodynamics*, *107–108*, 237–243.

Vino, G., Watkins, S., Mousley, P., Watmuff, J., & Prasad, S. (2005). Flow structures in the near-wake of the Ahmed model. *Journal of Fluids and Structures*, *20*(5), 673–695.

Wilcox, D. C. (1988). Multiscale model for turbulent flows. *AIAA Journal*, *26*(11), 1311–1320.

CURRICULUM VITAE

Ahmet Halil ORAN was born on August 26, 1995, in Mersin. He graduated from Hacı Zarife - Çelebi Aygar Anatolian High School in 2013 and enrolled in the Automotive Engineering Department of Mersin University in the same year. He graduated from Mersin University as an Automotive Engineer in May 2017. He received his master of science degree from the Automotive Engineer Department of Çukurova University in September 2020. He has been employed as a Design Engineer in the Body Module Department of Günsel between May 2018 and April 2020.